Response letter

We thank the editor and two Reviewers for the careful consideration of our work. Their constructive and thoughtful comments and suggestions led to a much improved and complete revision of the manuscript. In the revised paper, we have addressed all the comments formulated by the Reviewers by replying (in black) to their remarks (in blue). The line numbers in this rebuttal refer to the revised version of the manuscript.

Responses to comments by the editor

I thank the reviewers for their detailed reviews and the authors for their meticulous replies. I recommend that the authors submit a revised manuscript taking good care that all the comments of the reviewers are well addressed in the document. I accept the paper with minor revisions.

Our reply: We thank Prof. Hubert Savenije for your positive assessment of our work. In the revised manuscript, we have fully addressed all the comments raised by two reviewers.

Responses to comments by Prof. Mick van der Wegen

General comments:

Last weeks I read with great interest your work on inverse modeling to determine the waterdepth from hydrodynamic parameters such as tidal amplification and wave propagation. This is an intriguing technique with many potential and important applications. I am thinking of determining a representative bed level for 1D (morphodynamic) models of long tidal river systems (such as the Yangtze or Ganges) based on local water level observations, particularly usefull in (bed)data scarce environments.

The authors present a first step of such an inverse model since their model approach is based on (explicitly mentioned) assumptions like absence of river flow or head reflectance and a constant bed level in the model domain. The work presented is nice straighthforward and reads quite gently. The analysis makes use of earlier analytical methods to describe tidal propagation in estuarine systems based on few and easily derivable parameters such as estuarine shape and wave attenuation. The approach requires quite rough schematizations that may oversimplify local conditions but are

necessary to come to an analytical solutions that can explain tidal dynamics in a straightforward manner.

Our reply: We thank Prof. Mick van der Wegen for your very positive assessment of our work.

Major comments:

Here I address my major considerations:

- Figure 12 gives a depth development over time. How did you determine the observed depth? Is that depth constant along the transect that you consider? This is important since one of your assumptions is that the depth is constant along the transect and you could simply test this assumption from data.

Our reply: In order to determine the mean water depth of Lingdingyang Bay, in this study, we first collected bathymetric maps of the bay surveyed in 1965, 1974, 1989, 1998, 2009, and 2015 from the Guangzhou Maritime Safety Administration and China People's Liberation Army Navy Command Assurance Department of Navigation. The submarine contours and estuarine shorelines on these maps were digitalized to generate a 50 × 50 m digital elevation model (DEM) with kriging interpolation in ArcGIS 10.3 (see Fig. R1 below). The bathymetric benchmark was converted from the local lowest tidal level to the Pearl River datum. Subsequently, **mean annual water depths were calculated as the ratio of the estuarine volume to the planimetric area.**

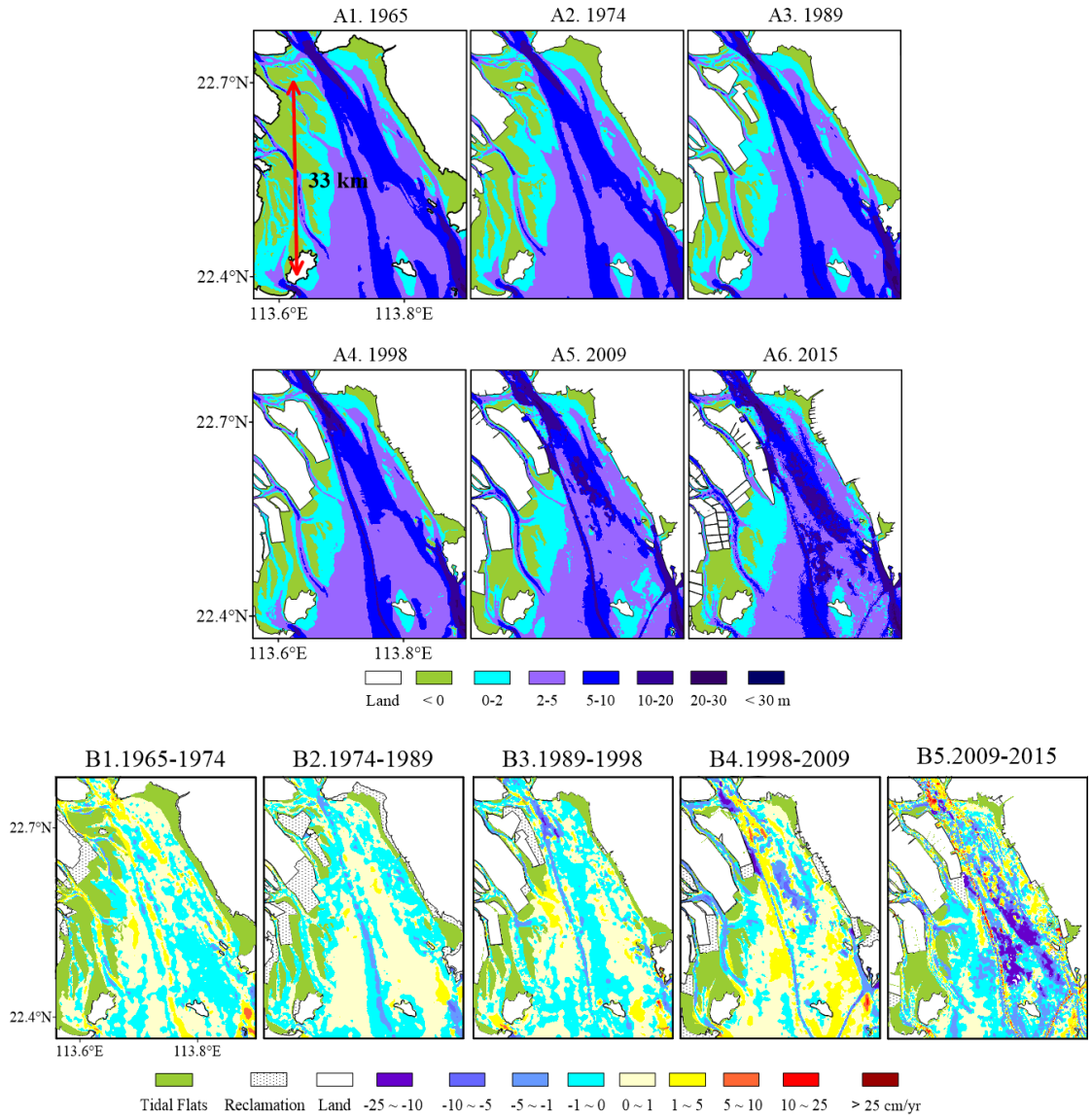

Fig. R1. Bathymetric maps of Lingdingyang Bay in 1965 (A1), 1974 (A2), 1989 (A3), 1998 (A4), 2009 (A5), and 2015 (A6) and its bathymetrical change rate during five time periods: 1965-1974 (B1), 1974-1989 (B2), 1989-1998 (B3), 1998-2009 (B4), and 2009-2015 (B5).

As can be seen from Fig. 8 in the manuscript (see also Fig. R2 below), the longitudinal water depth relative to the Pearl River datum is variable rather than constant. Here, in the inverse analytical model, it should be noted that the studied estuary was considered as an ensemble system, which is featured by a spatially averaged mean water depth and a channel width convergence length. Consequently, the estimated water depth in this work should be regarded as a bulk parameter for the system as a whole. In the section 2.2 of the revised manuscript, we have explicitly mentioned that "*In the inverse analytical model, it should be noted that the estuary is regarded as an ensemble system characterized by a spatially averaged water depth and a specific width convergence length.*" (see Lines 221-222)

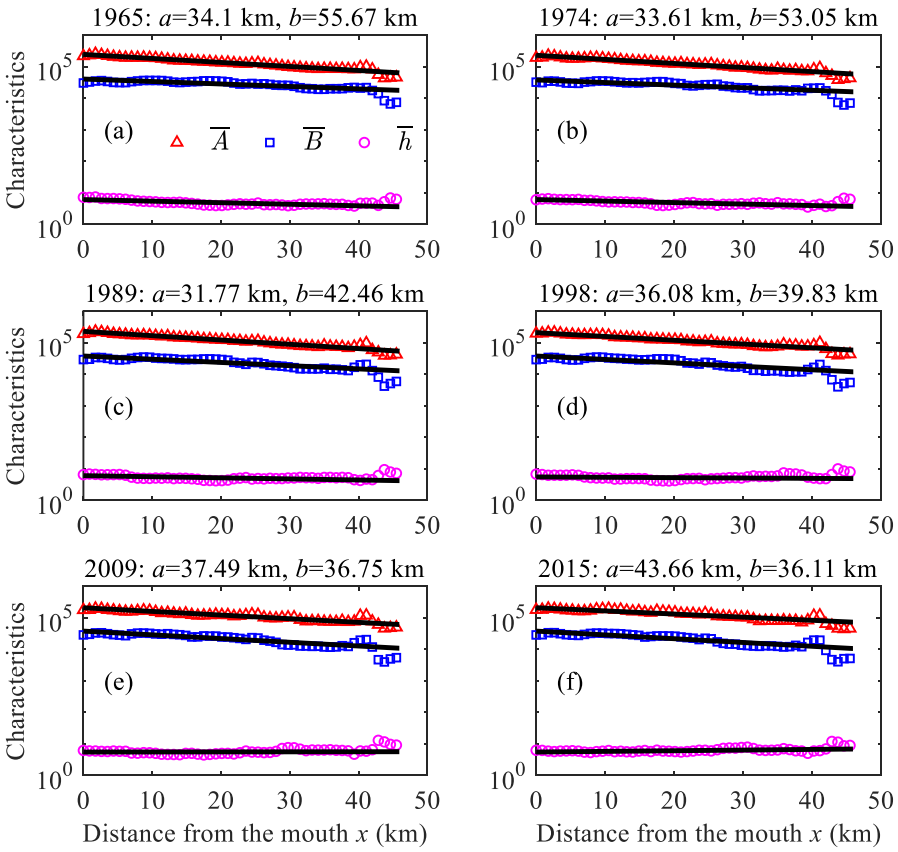

Fig. R2. Longitudinal variations of the geometric characteristics (the tidally averaged cross-sectional area $\bar{A}$, m^2, width $\bar{B}$, m, and depth $\bar{h}$, m) of Lingdingyang Bay for different years: a) 1965; b) 1974; c) 1989; d) 1998; e) 2009; and f) 2015, in which the black thin lines represent the best fitted curves according to the exponential functions (5)-(6).

-In line 351 you refer to the analytically computed tidal amplitude and phase. As far as I can oversee the equations the determination of the phase depends on the mean water depth, via eqs 9, 21 and 20. What water depth value did you use to determine the phase in figure 9? Is that the water depth determined in section 4.3?

Our reply: Here, in the forward analytical model we used a longitudinal variable mean water depth along the estuary. The water depth here is determined at each transverse cross section (see Fig. R2 above). In the revised manuscript, we shall clarify the adopted water depth in both the forward and the inverse analytical models. Specifically, in section 4.2 of the revised manuscript, we have explicitly mentioned in the model calibration process that: "*In order to account for the along-channel variations of the estuarine sections, we adopted a longitudinal variable depth along the channel.*" (see Lines 356-357)

- One of the assumptions that you implicitly make is that the tide in the Bay propagates along the channel. but is this actually true? Or does the tide propagate in a different way? You do not mention this, but I think it is important to note that explicitly.

Our reply: We thank the Reviewer for this comment. As we described in the study area part, Lingdingyang Bay is a funnel-shaped subaqueous delta and has a complicated geomorphology pattern with two deep channels (i.e., East and West Channels) between three shoals (i.e., East, Middle and West Shoals) (see Fig. 4c in the manuscript). From the energy point of view, it is true that the tide mainly propagates along the two deep channels, either during the flood tide or the ebb tide. In the analytical model, we consider the whole Lingdingyang Bay as an ensembled system. Thus, it is worth noting that in the analytical model the Manning-Stricker friction coefficient K should be regarded as an equivalent effective friction from the entire estuary, including the additional drag resistance due to bed forms, the influence of suspended sediments and the possible effect due to lateral storage areas (Cai et al., 2016). Hence, in the revised manuscript, we have explicitly mentioned that: "*In addition, it is worth noting that in the analytical model the calibrated Manning-Stricker friction coefficient K should be regarded as an equivalent effective friction coefficient induced by the entire estuary, including the additional drag resistance due to bed forms, the influence of suspended sediments and the possible effect due to lateral storage areas (Cai et al., 2016).*" (see Lines 365-368)

Minor comments:

1. Line61: "for an infinitely long channel" better move to lines 64-72 wger other restrictions/assumptions are mentioned

Our reply: Revised as suggested. In the revised manuscript, we have explicitly mentioned that: "*Here, we restrict consideration to infinitely long tide-dominated estuaries with small tidal amplitude to depth ratios and Froude numbers.*" (see Lines 64-66)

2. Lines 62-74: better move to section 2.1

Our reply: Here we would like to clarify the analytical method adopted and the related assumptions since analytical method usually requires a certain number of assumptions with regard to geometry and flow characteristics. Hence, we would keep this paragraph at the same place.

3. Lines 73-86: better summarize here in 1-2 sentences and move the rest to section 3.1

Our reply: Here we would like to briefly introduce the study area and to highlight the contribution made from this study. In the revised manuscript, we have explicitly mentioned that: "*The Pearl River is the second largest river in terms of water discharge in China (Liu et al., 2017) and drains into the South China Sea through Lingdingyang Bay, Modaomen Estuary and Huangmaohai Bay.* ***In this study, we focus on Lingdingyang Bay, which is the largest of these tidal systems in terms of water area and consists of three major shoals and two channels.***" (see Lines 74-75)

4. Line 77: "is constituted by three"→ "consists of three major"

Our reply: Revised as suggested.

5. Line 77 and Line 82: "troughs"→ "channels"

Our reply: Revised as suggested.

6. Line 146: pls indicate what eta stands for

Our reply: The definition of η was provided when introducing the Equation (7).

7. Line 200: "nor"→ "or"

Our reply: Revised as suggested.

8. Line201: "then" removed

Our reply: Revised as suggested.

9. Line212: “is decreased”→ “decreases”

Our reply: Revised as suggested.

10. Line 238: “come”→ “comes”

Our reply: Revised as suggested.

11. Lines 242-243: “owing to its dramatic volume for water bodies” removed

Our reply: Revised as suggested.

12. Line 280: at some instances throughout the text you provide only a nr; better state "equation (26)" than only "(26)". pls check other parts of the text as well

Our reply: Revised as suggested.

13. Line 294: “the”→ “a”

Our reply: Revised as suggested.

14. Line 302: “; however”→ “. However”

Our reply: Revised as suggested.

15. Line 316: “are decreased”→ “decrease”

Our reply: Revised as suggested.

16. Line 333: “is increased”→ “increases”

Our reply: Revised as suggested.

17. Line 336: “that” removed

Our reply: Revised as suggested.

18. Line 350: “greater”→ “larger”

Our reply: Revised as suggested.

19. Line 360: “the”→ “a”

Our reply: Revised as suggested.

20. Line 361: “the”→ “a”

Our reply: Revised as suggested.

21. Line 413: “shows”→ “has shown”

Our reply: Revised as suggested.

22. Line 414: “; therefore”→ “. Therefore”

Our reply: Revised as suggested.

23. Line 430: “which”→ “This”

Our reply: Revised as suggested.

24. Figure 6: it would be nice to see a km scale here two to get a sense of size

Our reply: Revised as suggested (see Fig. R1 above).

25. Figure 8: the symbols are not recognizable in the figures; better use a coloured line or so

Our reply: Revised as suggested (see Fig. R2 above).

26. Figure 11: IN between the two figure columns the y axis legends are intervening like there is a parameter H/h. Maybe put the figures more apart

Our reply: Revised as suggested (see Fig. R3 below).

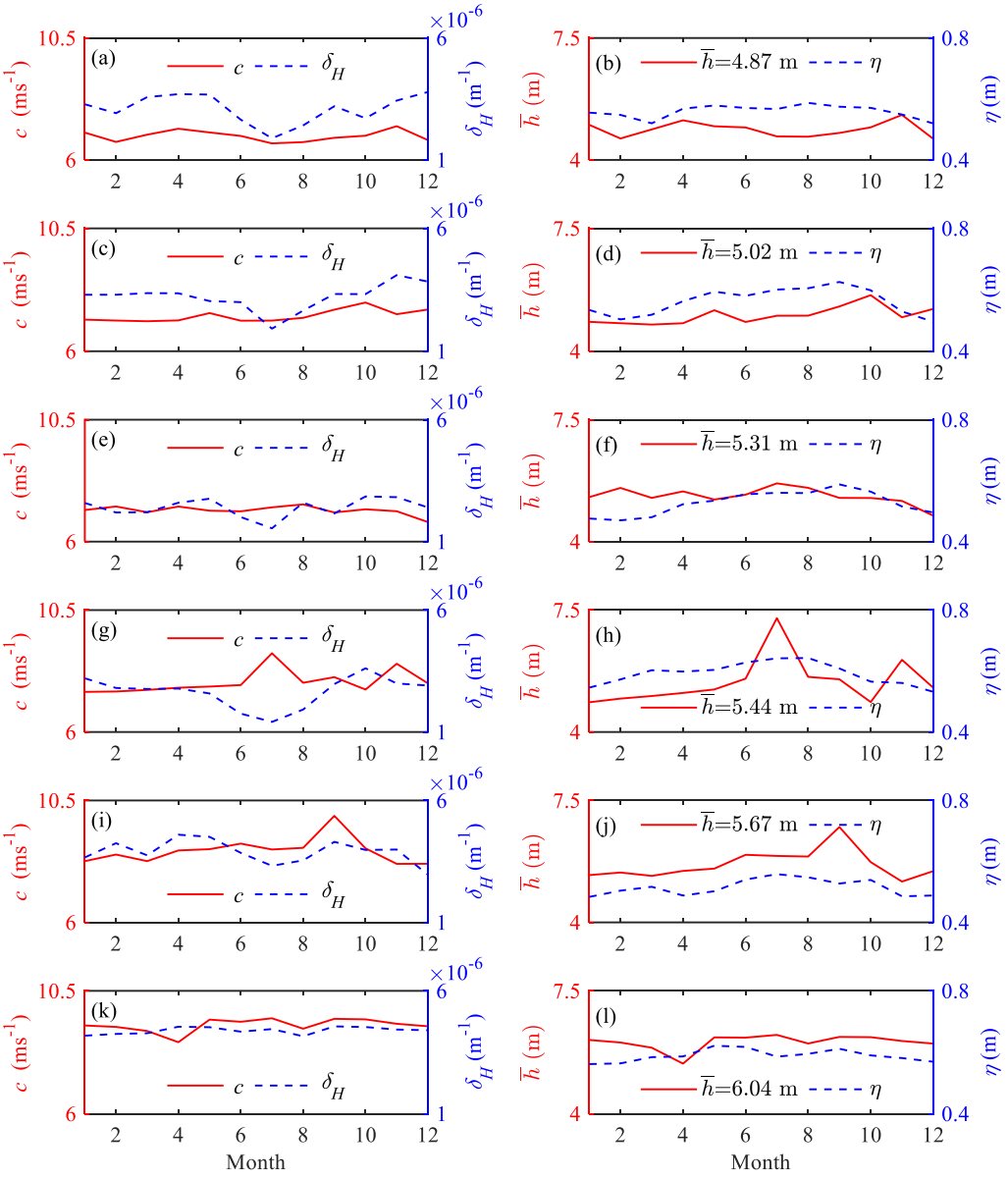

Fig. R3. Estimation of the tidally averaged depth $\overline{h}$ (the right panels, together with the tidal amplitude at the CW station η) using observed wave celerity c and tidal damping/amplification rate δ_H (the left panels) for different years: 1965 (a, b), 1974 (c, d), 1989 (e, f), 1998 (g, h), 2009 (i, j) and 2015 (k, l).

Responses to comments by Reviewer#2

General comments:

The paper presented a new analytical 1D approach to estimate the changes of morphological characteristics such as the tidally average depth, wave celerity and tidal amplification in an estuary. Despite of the assumptions made with the absence of river

flow and a constant depth in the inverse model, this finding provides a useful and yet simple tool to obtain a first estimation of the morphological changes. Furthermore, it is applicable to be applied in region where minimal data is available.

The manuscript is well-organized, and the data and results are well-presented. There are few typos and grammatical error spotted but they are only minor. Nevertheless, there are some unclear sections that I would like to address in my comments below:

Our reply: We thank the reviewer for his/her overall positive assessment of our work.

Major comments:

1. Page 8, paragraph 1, Figure 3: Authors mentioned with $r_S = 1$, Equation (25) indicates that the tidally averaged depth varies proportionally with the tidal damping rate δ_H. However, in Figure 3 the different colours shades representing the changes in averaged depth only varies with the celerity (vertically) and not the tidal damping rate (horizontally). Also, there is no indication on which point or region the depth is minimum and tidal damping is at critical condition. Authors are recommended to revised on this section.

Our reply: We very much appreciate the reviewer's comment and advice. Generally, the storage width ratio r_S ranges between 1 and 2 (Savenije, 2005). In Figure 3, for illustration, we assume that r_S=1. Actually, it can be seen from Equation (25) that the relationship between tidally averaged depth $\bar{h}$ and the tidal damping (or amplification) rate δ_H is nonlinear. To highlight such a kind of nonlinear relationship, in the revised manuscript, we have provided the derivatives of the tidally averaged depth with respect to two variables (i.e., the wave celerity and the tidal damping or amplification rate):

$$\frac{\partial \bar{h}}{\partial c} = \frac{2r_S b^2 c\omega^4}{g\left(\delta_H c^2 - \delta_H^2 c^2 b + b\omega^2\right)^2} \quad \text{(R1)}$$

$$\frac{\partial \bar{h}}{\partial \delta_H} = \frac{r_S b c^4 \left(2\delta_H b - 1\right)}{g\left(\delta_H c^2 - \delta_H^2 c^2 b + b\omega^2\right)^2} \quad \text{(R2)}$$

It can be seen from Equation (R1) that the depth $\bar{h}$ tends to increase with the celerity c since the value of $\partial\bar{h}/\partial c$ is always positive. On the other hand, it can be seen from Equation (R2) that the depth $\bar{h}$ is decreased with the tidal damping (or amplification) rate δ_H until a minimum value is reached at a critical δ_H corresponding to the condition $\partial\bar{h}/\partial\delta_H = 0$, i.e., δ_H=1/(2b). A further increase of the δ_H yields an increase of $\bar{h}$. In the revised manuscript, we have updated the original Fig. 3 by including the critical value of δ_H=1/(2b) (see Fig. R4 below).

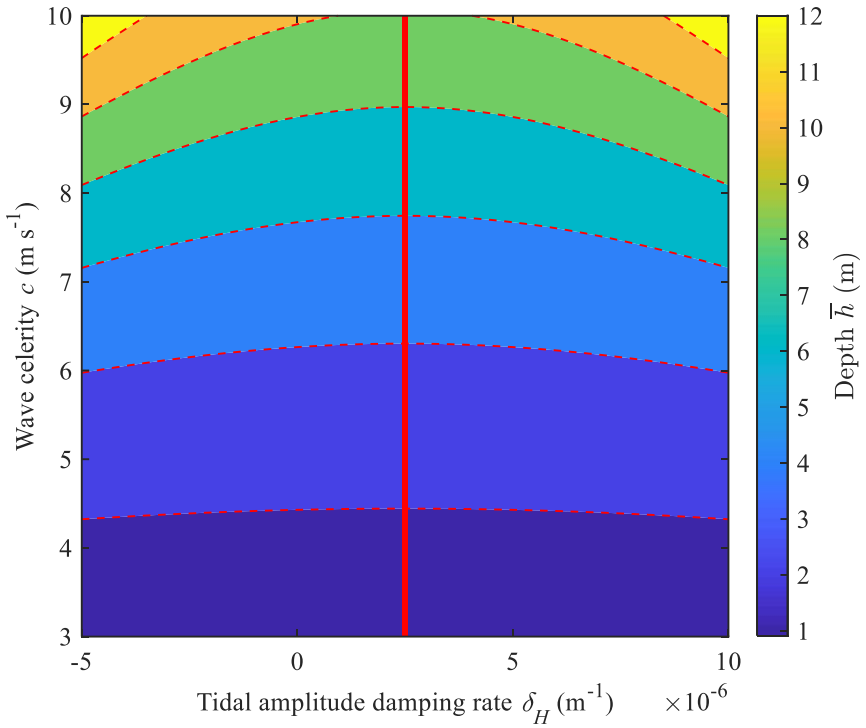

Fig. R4. Contour plot of the estimated depth $\bar{h}$ as a function of the wave celerity c and tidal amplitude damping (or amplification) rate δ_H obtained from Equation (22). The drawn red line indicates the critical value of δ_H=1/(2b) corresponding to the minimum water depth for a given constant wave celerity.

2. Section 4.1: The definition of tidal damping/amplification rate is confusing. Does the (/) means "or" or ratio? In line 312, it is mentioned that the tidal damping/amplification rate can be compute with Equation (27) and has the symbol δ_H. But, in line 317 there is another symbol representing the tidal damping/amplification rate which is β. In Figure 7, both symbols are presented with different indication, and is the gradient of the regression between the tidal amplification and tidal amplitude. What does the gradient means in this context? The same issue also goes to the wave celerity. Also, it would be nice if the authors can explain more clearly on how the negative gradient indicating stronger amplification and faster celerity during neap tide than spring tide.

Our reply: Here tidal damping/amplification rate means tidal damping rate (δ_H<0) or tidal amplification rate (δ_H≥0). In the revised manuscript, we have replaced "tidal damping/amplification" with "*tidal damping (or amplification)*". Actually, the gradient β indicates the change rate of the tidal damping/amplification rate δ_H with respect to the tidal amplitude at the estuary mouth η_0, where smaller values indicate the periods for the neap tide, while larger values indicate the periods for the spring tide. Hence the negative gradient (β<0) suggests that the value of δ_H is decreased with the increasing tidal amplitude, which means stronger tidal amplification for the neap tide (smaller η_0, larger δ_H) than that for the spring tide (larger η_0, smaller δ_H). Similarly, the negative

gradient α for the wave celerity indicates a faster wave celerity for the neap tide (smaller η_0, larger c) than that for the spring tide (larger η_0, smaller c). In the revised manuscript, we have clarified that: "*In general, we observe that both wave celerity and the damping (or amplification) rate decrease with increasing tidal amplitude at the estuary mouth with slightly different negative slopes (indicated by α and β representing the change rate of wave celerity and tidal damping or amplification rate with respect to the tidal amplitude, respectively), suggesting a more strongly amplified yet faster wave for the neap tide (smaller η_0, larger δ_H and c) than for the spring tide (larger η_0, smaller δ_H and c).*" (see Lines 322-327)

3. Section 4.3: In Equation (25), $r_S = 1$ was used for analysis. In this section, the values used for r_S were calibrated against observed data using the shape preserving piecewise cubic interpolation in which the results are presented in Table 3. From the table, the values of r_S obtained is close unity. It would be more interesting if the calibration process in obtaining of the r_S values can be explained further showing in what sense the values are near to 1.

Our reply: In the revised manuscript, we shall explicitly clarify that the storage width ratio r_S generally ranges between 1 and 2 (Savenije, 2005). In Figure 3, we adopted a constant value of $r_S = 1$ for simplification. With regard to calibration, in the revised manuscript, we have clarified the process of determining the value of r_S: "*We calibrated the analytical model by adjusting the Manning-Strickler friction coefficient K and the storage width ratio r_S, which are detailed in Table 3.* ***In particular, the calibrated r_S is relatively sensitive to the variation in phase of the elevation. In addition, it is worth noting that in the analytical model the calibrated Manning-Stricker friction coefficient K should be regarded as an equivalent effective friction coefficient induced by the entire estuary, including the additional drag resistance due to bed forms, the influence of suspended sediments and the possible effect due to lateral storage areas (Cai et al., 2016).*** *The model performance was evaluated by the root mean squared error (RMSE), where RMSE=0 corresponds to perfect agreement. In general, the correspondence between analytical results and observations is good, both for the tidal amplitude (with RMSE ranging between 0.015 and 0.020 m) and the phases (with RMSE ranging between 1.1° and 2.1°), suggesting that the analytical model can reproduce the main tidal hydrodynamics in Lingdingyang Bay well. The calibrated friction coefficient K ranges between 58 $m^{1/3}s^{-1}$ and 90 $m^{1/3}s^{-1}$, with a minimum value occurring in 2009 (indicating relatively strong friction) and a maximum in 1965 (indicating relatively weak friction).* ***On the other hand, the calibrated storage width ratio r_S is approximately unit (ranging between 1.0 and 1.15), which suggests a minor impact from the lateral storage areas on the evolution of tidal hydrodynamics.***" (see Lines 362-377)

4. Figure 8: It would be nice if the authors can include the values of the geometry characteristics in this figure for each year. The lines could not show clear difference in the geometry changes over the years and look almost the same. With the geometry characteristics values included, it is easier to see how much the geometry has changed.

Our reply: We agree with the reviewer's comment. In the revised manuscript, we have updated the Fig. 8 (see Fig. R2 above).

References:

Cai, H., Toffolon, M., and Savenije, H. H. G.: An analytical approach to determining resonance in semi-closed convergent tidal channels, Coastal Engineering Journal, 58, 1650 009, doi:Artn 165000910.1142/S0578563416500091, 2016.

Savenije, H. H. G.: Salinity and Tides in Alluvial Estuaries, Elsevier, New York, 2005.

Manuscript prepared for Hydrol. Earth Syst. Sci.
with version 5.0 of the LaTeX class copernicus.cls.
Date: 12 March 2020

A novel approach for the assessment of morphological evolution based on observed water levels in tide-dominated estuaries

Huayang Cai[1,2], Ping Zhang[1,2], Erwan Garel[3], Pascal Matte[4], Shuai Hu[1,2], Feng Liu[1,2], and Qingshu Yang[1,2]

[1]Institute of Estuarine and Coastal Research/State and Local Joint Engineering Laboratory of Estuarine Hydraulic Technology, School of Marine Engineering and Technology, Sun Yat-sen University, Guangzhou, China
[2]Guangdong Provincial Engineering Research Center of Coasts, Islands and Reefs/Southern Marine Science and Engineering Guangdong Laboratory (Zhuhai), Zhuhai, China
[3]Centre for Marine and Environmental Research (CIMA), University of Algarve, Portugal
[4]Meteorological Research Division, Environment and Climate Change Canada, Quebec, Canada

Correspondence to: Feng Liu (liuf53@mail.sysu.edu.cn)

Abstract. Assessing the impacts of both natural (e.g., tidal forcing from the ocean) and human-induced changes (e.g., dredging for navigation, land reclamation) on estuarine morphology is particularly important for the protection and management of the estuarine environment. In this study, a novel analytical approach is proposed for the assessment of estuarine morphological evolution in terms of tidally averaged depth on the basis of the observed water levels along the estuary. The key lies in deriving a relationship between wave celerity and tidal damping or amplification. For given observed water levels at two gauging stations, it is possible to have a first estimation of both wave celerity (distance divided by tidal travelling time) and tidal damping or amplification rate (tidal range difference divided by distance), which can then be used to predict the morphological changes via an inverse analytical model for tidal hydrodynamics. The proposed method is applied to the Lingdingyang Bay of the Pearl River Estuary, located on the southern coast of China, to analyse the historical development of the tidal hydrodynamics and morphological evolution. The analytical results show surprisingly good correspondence with observed water depth and volume in this system. The merit of the proposed method is that it provides a simple approach for understanding the decadal evolution of the estuarine morphology through the use of observed water levels, which are usually available and can be easily measured.

1 Introduction

Understanding the morphological changes in estuaries due to natural processes and human interventions is especially important with regard to sustainable water management and ecological impacts on the estuarine environment (Prandle, 2004; Schuttelaars et al., 2013; Winterwerp and Wang, 2013; Wang et al., 2015; Hoitink et al., 2017; Luan et al., 2017). In recent decades, human activities have been crucial factors affecting the morphological evolution in estuaries, and morphological responses of estuaries to human activities have attracted worldwide attention (Syvitski et al., 2009; Monge-Ganuzas et al., 2013; Du et al., 2016; van Maren et al., 2016; Jiang et al., 2017). In previous studies, aerial photographs, satellite images, topographic maps and cross-sectional profiles are the commonly used field data to explore the morphological adjustments with varied resolution and accuracy by means of either data-driven studies (e.g., Zhang et al., 2015; Wu et al., 2014, 2016a,b) or process-based morphodynamic models (e.g., Guo et al., 2014, 2016; Luan et al., 2017). It is noted that these high-resolution and successive field data are rare or unavailable in most estuaries, especially because the determination of detailed morphological changes is usually time and energy consuming. Hence, the development of a simple yet effective approach for the assessment of decadal morphological evolution without the need for bathymetric data collection is desirable, which is especially the case for ungauged basins (Gisen and Savenije, 2015).

In a frictionless, prismatic channel of a constant cross-section (or an ideal estuary with no damping or amplification), the classical formula for tidal wave propagation can be described by (e.g., Savenije, 2012):

$$c_0 = \sqrt{g\overline{h}/r_S}\,, \tag{1}$$

where c_0 is the classical wave speed, g is the acceleration due to gravity, $\overline{h}$ is the tidally averaged and cross-sectionally averaged water depth, and r_S is the storage width ratio accounting for the intertidal storage in tidal flats or marshes. Thus for a frictionless, prismatic channel or an ideal estuary, it is possible to derive an analytical expression for the stream depth, i.e., $\overline{h} = r_S c_0^2/g$, which is proportional to the square of the classical wave speed (Savenije and Veling, 2005). However, Equation (1) does not apply in real alluvial estuaries due to the predominance of either morphological convergence or bottom friction. Thus, to have a first-order estimate of the stream depth, a relationship taking into account both tidal damping (or amplification) and channel convergence should be adopted. Such a relationship can be easily obtained from the recently published analytical solutions for tidal hydrodynamics in convergent estuaries (e.g., Savenije and Veling, 2005; Savenije et al., 2008; Toffolon and Savenije, 2011; van Rijn, 2011; Cai et al., 2012, 2016; Winterwerp and Wang, 2013).

Previous studies have clearly demonstrated that the behaviour of both the tidal damping ~~/amplification~~(or amplification) and wave speed strongly depends on the degree of channel con-

vergence and on the intensity of friction (e.g., Jay, 1991; Savenije and Veling, 2005). In particular, analytical solutions of tidal hydrodynamics are able to predict the main trends of tidal damping ~~/amplification~~(or amplification) and wave speed for given forcing tidal amplitude, geometry (e.g., the spatially averaged depth and width convergence length) and friction (e.g., Prandle and Rahman, 1980; Friedrichs and Aubrey, 1994; Savenije et al., 2008; Toffolon and Savenije, 2011; van Rijn, 2011; Cai et al., 2012, 2016; Winterwerp and Wang, 2013). Conversely, if tidal damping ~~/amplification~~(or amplification) and wave speed are known from observations, analytical models can be used to estimate the unknown tidally averaged depth and other tidal dynamics (e.g., velocity amplitude, phase difference between velocity and elevation, etc.). Following this line of thought, the main objective of this study is to provide an analytical framework ~~(for an infinitely long channel)~~ to assess the morphological evolution of estuaries based on the tidally averaged depth derived from the observed tidal hydrodynamics (i.e., tidal damping ~~/~~or amplification and wave speed).

It is worth noting that considerable simplifications of geometry and forcing are made in order to derive generic analytical solutions of the governing St. Venant equations. Here, we restrict consideration to infinitely long tide-dominated estuaries with small tidal amplitude to depth ratios and Froude numbers. The fundamental assumption is that the geometry (cross-sectional area, width and depth) of the channel can be described by a simple exponential function. We also assume that the velocity of river discharge is small compared to the tidal velocity. In this paper, we use the analytical relation of wave celerity, first proposed by Savenije and Veling (2005), to predict the estuarine morphological dynamics in terms of the large-scale geometrical properties of the estuary, i.e., the tidally averaged depth and volume based on the observed water levels through the estuary.

The Pearl River is the second largest river in terms of water discharge in China (Liu et al., 2017) and drains into the South China Sea through Lingdingyang Bay, Modaomen Estuary and Huangmaohai Bay. ~~Among these three outer bays, Modaomen estuary carries the largest portion of freshwater discharge (Gong and Shen, 2011), while Lingdingyang Bay~~In this study, we focus on Lingdingyang Bay, which is the largest of these tidal systems in terms of water area and ~~is constituted by three~~ consists of three major shoals and two ~~troughs~~channels. Previous studies have examined the morphological evolution of Lingdingyang Bay using satellite images (e.g., Wu et al., 2014), topographic maps (e.g., Wu et al., 2016a,b) and cross-sectional profiles (Wu et al., 2016b). Due to intensive human activities (e.g., land reclamation and channel dredging), significant morphological changes have occurred in Lingdingyang Bay in recent decades. As a consequence, the West and East shoals expanded towards the bay, and the two troughs became narrower and deeper (Zhang et al., 2015; Wu et al., 2016b). Furthermore, these morphological changes have resulted in changes in tidal dynamics (Zhang et al., 2010; Deng and Bao, 2011). Our study can provide a new method to explore the morphological evolution, which provides scientific guidelines for management and regulation projects in estuaries.

The paper is organized as follows. Section 2 describes the analytical method for reproducing the

tidal hydrodynamics and an inverse model for predicting the tidally averaged depth. An overview of the study area is provided in section 3. In section 4, the morphological evolution of Lingdingyang Bay is described, and the proposed method is applied. Subsequently, the relationship between morphology and tidal dynamics are discussed, along with the model limitations (section 5). Finally, some conclusions are drawn in section 6.

2 Methodology and material

2.1 Analytical model for tidal hydrodynamics in an infinitely long channel

Neglecting the nonlinear continuity term $\partial h/\partial x$ and the advective term $U\partial U/\partial x$, the linearized depth-averaged equations for the conservation of mass and momentum in a channel with a gradually varying cross-section can be described by (e.g., Savenije, 2005; van Rijn, 2011):

$$r_S \frac{\partial Z}{\partial t} + U\frac{\partial Z}{\partial x} + h\frac{\partial U}{\partial x} + \frac{hU}{\overline{B}}\frac{\mathrm{d}\overline{B}}{\mathrm{d}x} = 0\,, \tag{2}$$

$$\frac{\partial U}{\partial t} + U\frac{\partial U}{\partial x} + g\frac{\partial Z}{\partial x} + \frac{rU}{h} = 0\,, \tag{3}$$

where U is the cross-sectionally averaged velocity, Z is the free surface elevation, h is the water depth, $\overline{B}$ is the tidally averaged width (hereafter, overbars denote tidal averages), t is the time, x is the longitudinal coordinate measured positive in landward direction (x=0 at the mouth), and r is the linearized friction factor defined by (Lorentz, 1926):

$$r = \frac{8}{3\pi}\frac{g\upsilon}{K^2\bar{h}^{1/3}}\,, \tag{4}$$

where the coefficient $8/(3\pi)$ stems from adopting Lorentz's linearization of the quadratic friction term (Lorentz, 1926) considering only one single predominant tidal constituent (e.g., M_2), and K is the Manning-Strickler friction coefficient.

To derive the analytical solution for the tidal hydrodynamics in convergent channels, it is assumed that the tidally averaged cross-sectional area $\overline{A}$ and width $\overline{B}$ can be described by the following exponential functions:

$$\overline{A} = \overline{A_0}\exp\left(-x/a\right)\,, \tag{5}$$

$$\overline{B} = \overline{B_0}\exp\left(-x/b\right)\,, \tag{6}$$

where $\overline{A_0}$ and $\overline{B_0}$ are the respective values at the estuary mouth and a and b are the convergence lengths of the cross-sectional area and width, respectively. The other fundamental assumption is that the flow is mainly concentrated in a rectangular cross-section, with a possible influence from

storage areas described by the storage width ratio r_S. It directly follows from the assumption of a rectangular cross-section that the tidally averaged depth is given by $\overline{h} = \overline{A}/\overline{B}$.

Considering a system that is forced by a sinusoidal tidal wave with period T and frequency $\omega = 2\pi/T$, the wave functions of water level and flow velocity are defined as:

$$Z = \eta \cos(\omega t - \phi_Z) \,, \tag{7}$$

$$U = \upsilon \cos(\omega t - \phi_U) \,, \tag{8}$$

where η and υ are the wave amplitudes of elevation and velocity, while ϕ_Z and ϕ_U are their corresponding phases. As the wave propagates into the estuary, it has a wave celerity c and a phase lag ε, defined as the phase difference between high water (HW) and high water slack (HWS) (or between low water (LW) and low water slack (LWS)). For a simple harmonic wave, $\varepsilon = \pi/2 - (\phi_Z - \phi_U)$. After scaling Equations (2) and (3) (see details in Appendix A), five dimensionless variables can be derived: the estuary shape number γ (representing the effect of cross-sectional area convergence), the friction number χ (describing the role of frictional dissipation), the velocity number μ (the actual velocity scaled with the frictionless value in a prismatic channel), the celerity number λ (the ratio between the theoretical frictionless celerity in a prismatic channel and the actual wave celerity), and the damping number for tidal amplitude δ (a dimensionless description of the increase, $\delta > 0$, or decrease, $\delta < 0$, of the tidal wave amplitude along the estuary), where γ and χ are the independent variables, while μ, λ, δ (together with ε) are the dependent variables. These dimensionless variables are defined as:

$$\gamma = \frac{c_0}{\omega a} \,, \tag{9}$$

$$\chi = r_S f \frac{c_0}{\omega} \zeta \,, \tag{10}$$

$$\mu = \frac{1}{r_S} \frac{\upsilon \overline{h}}{\eta c_0} \,, \tag{11}$$

$$\lambda = \frac{c_0}{c} \,, \tag{12}$$

$$\delta = \frac{1}{\eta} \frac{\mathrm{d}\eta}{\mathrm{d}x} \frac{c_0}{\omega} \,, \tag{13}$$

where f is the dimensionless friction factor, and ζ is the dimensionless tidal amplitude defined as:

$$f = \frac{g}{K^2 \overline{h}^{1/3}} \left(1 - (1.33\zeta)^2\right)^{-1} \,, \tag{14}$$

$$\zeta = \frac{\eta}{\overline{h}} \,. \tag{15}$$

Making use of these dimensionless parameters, Cai et al. (2012), building on the previous work by Savenije et al. (2008), showed that the analytical solution of the tidal hydraulic equations can be obtained by solving a set of four implicit equations, i.e., the phase lag Equation (16), the scaling Equation (17), the damping Equation (18) and the celerity Equation (19):

$$\tan(\varepsilon) = \frac{\lambda}{\gamma - \delta}, \tag{16}$$

$$\mu = \frac{\sin(\varepsilon)}{\lambda} = \frac{\cos(\varepsilon)}{\gamma - \delta}, \tag{17}$$

$$\delta = \frac{\gamma}{2} - \frac{4\chi\mu}{3\pi\lambda}, \tag{18}$$

$$\lambda^2 = 1 - \delta(\gamma - \delta). \tag{19}$$

In addition, the solutions for the phases of elevation and velocity are given by (see details in Cai et al., 2016):

$$\tan(\phi_Z) = \frac{\Im(A^*)}{\Re(A^*)}, \quad \tan(\phi_U) = \frac{\Im(V^*)}{\Re(V^*)}, \tag{20}$$

where $\Re$ and $\Im$ are the real and imaginary parts of the corresponding term and A^* and V^* are complex functions of amplitudes that vary along the dimensionless coordinate $x^* = x/(c_0 T)$ as follows:

$$A^* = \exp[2\pi(\gamma/2 - \Lambda)x^*], \quad V^* = \frac{i}{\Lambda + \gamma/2}\exp[2\pi(\gamma/2 - \Lambda)x^*], \tag{21}$$

where i is the imaginary unit, and Λ is a complex variable defined as:

$$\Lambda = \sqrt{\frac{\gamma^2}{4} - 1 + i\frac{8}{3\pi}\mu\chi}. \tag{22}$$

It is worth considering the solution in the special case of an ideal estuary (with no damping or amplification $\delta = 0$) since natural estuarine systems tend to reach an equilibrium state of ideal estuaries. By imposing $\delta = 0$ in the set of Equations (16)-(19), one can easily obtain:

$$\delta = 0, \quad \lambda = 1, \quad \mu = \frac{1}{\sqrt{\gamma^2 + 1}}, \quad \tan(\varepsilon) = \frac{1}{\gamma}. \tag{23}$$

Figure 1 shows the variation of the four dimensionless parameters as a function of γ and χ obtained by solving Equations (16)-(19). The thick red lines indicate the values for the special case of an ideal estuary, which follows directly from Equation (23).

It is important to note that the analytical solutions of the linear model are local because they depend only on local (fixed position) quantities (i.e., the local tidal amplitude to depth ratio ζ, the local estuary shape number γ and the local friction number χ). To follow along-channel variations of these local variables, a multi-reach approach (subdividing the whole estuary into short reaches) has been used, in which the damping number δ is integrated in short reaches over which the estuary shape number γ and the friction number χ are assumed to be constant. This is done by using simple explicit integration of the linear differential equation (Savenije et al., 2008):

$$\eta_1 = \eta_0 + \frac{\mathrm{d}\eta}{\mathrm{d}x}\Delta x = \eta_0 + \frac{\delta \eta_0 \omega \Delta x}{c_0}, \tag{24}$$

where η_0 is the tidal amplitude at the origin of the axis for every short reach, while η_1 the tidal amplitude at a distance Δx (e.g., 1 km) upstream.

2.2 Estimation of the tidally averaged depth

To address directly the correspondence between tidal dynamics and morphology, the celerity Equation (19) proposed by Savenije and Veling (2005) is considered. This analytical relationship is an extension of the classical celerity equation for a progressive wave in a frictionless prismatic channel and depicts the along-channel wave celerity ($\lambda = c_0/c$) as a function of the tidal damping (δ) and estuary shape number (γ), hence accounting implicitly for the water depth (see Equation 9). Figure 2 shows the analytically computed λ^2 over a wide range of values of δ, from -3 to 1, and γ, from 0 to 4, directly from Equation (19). It can be clearly seen from Figure 2 that there exist two distinct types of estuaries characterized by the threshold of $\delta = 0$. For positive values of δ (amplified estuary), $\lambda < 1$, since the actual wave celerity c is larger than the classical one c_0, while it is the opposite ($\lambda > 1$) for negative values of δ (damped estuary). The underlying mechanism lies in the imbalance between channel convergence and bottom friction (i.e., stronger impact of convergence than friction in the case of amplification, and the opposite in the case of damping). Without damping ~~nor~~ or amplification ($\lambda = 1$, indicating balance between convergence and friction), ~~then~~ the estuary corresponds to an ideal estuary, where the wave celerity equals c_0. Interestingly, according to Equation (19), for an amplified estuary ($\delta > 0$), the actual wave celerity c could equal to c_0 for the special case of $\gamma = \delta$, which is due to the balance between channel convergence and acceleration effects (Jay, 1991).

Estimation of the tidally averaged depth $\overline{h}$ can be derived analytically by rewriting Equation (19) in terms of the width convergence length b, wave celerity c and tidal ~~amplitude damping~~ damping (or amplification) rate δ_H, which leads to (see details in Appendix B):

$$\overline{h} = \frac{r_S b c^2 \omega^2}{g\left(\delta_H c^2 - \delta_H^2 c^2 b + b\omega^2\right)}. \tag{25}$$

~~Figure 3 illustrates the analytically computed depth with Equation as a function of the wave celerity c and tidal amplitude damping rate δ_H for a constant width convergence length b=200 km~~

~~and storage width ratio r_S=1. It can be seen that the depth $\overline{h}$ tends to increase with the celerity c. On the other hand, the depth $\overline{h}$ is decreased with the tidal damping rate δ_H until a minimum value is reached at a critical δ_H corresponding to the condition $\partial\overline{h}/\partial\delta_H = 0$. A further increase of the δ_H yields an increase of $\overline{h}$. The~~ Here, the wave celerity c and the tidal ~~amplitude damping~~ damping (or amplification) rate δ_H can be estimated for a reach of Δx:

$$c = \frac{c_{HW} + c_{LW}}{2} = \frac{\Delta x}{2}\left(\frac{1}{\Delta t_{HW}} + \frac{1}{\Delta t_{LW}}\right), \tag{26}$$

$$\delta_H = \frac{1}{(\eta_1 + \eta_2)/2}\frac{\eta_2 - \eta_1}{\Delta x}, \tag{27}$$

where c_{HW} and c_{LW} are the wave celerity for high water (HW) and low water (LW), Δt_{HW} and Δt_{HW} are the corresponding travelling times over the reach, η_1 is the tidal amplitude in the seaward part, and η_2 is the tidal amplitude Δx upstream. The wave celerity c can also be estimated through harmonic analysis. In this case, Equation (26) can be rewritten as

$$c = \frac{\Delta x}{(\phi_{Z2} - \phi_{Z1})T/360}, \tag{28}$$

where ϕ_{Z1} is the phase of elevation at the seaward station, while ϕ_{Z2} is the corresponding values at Δx upstream. As illustrated in the next section, these parameters can be easily obtained from tidal gauge observations, providing a simple means to quickly assess the mean water depth with Equation (25).

In the inverse analytical model, it should be noted that the estuary is regarded as an ensemble system characterized by a spatially averaged water depth and a specific width convergence length. Based on the analytical expression of tidally averaged depth (Equation 25), the variations of depth with two variables (i.e., the wave celerity and the tidal damping or amplification rate) can be further explored by using the following derivatives:

$$\frac{\partial\overline{h}}{\partial c} = \frac{2r_S b^2 c\omega^4}{g\left(\delta_H c^2 - \delta_H^2 c^2 b + b\omega^2\right)^2}, \tag{29}$$

$$\frac{\partial\overline{h}}{\partial\delta_H} = \frac{r_S b c^4\left(2\delta_H b - 1\right)}{g\left(\delta_H c^2 - \delta_H^2 c^2 b + b\omega^2\right)^2}, \tag{30}$$

Figure 3 illustrates the analytically computed depth with Equation (25) as a function of the wave celerity c and tidal damping (or amplification) rate δ_H for a constant width convergence length b=200 km and storage width ratio r_S=1. It can be seen that the depth $\overline{h}$ tends to increase with the celerity c since the value of $\partial\overline{h}/\partial c$ is always positive (see Equation 29). On the other hand, the depth $\overline{h}$ decreases with the tidal damping (or amplification) rate δ_H until a minimum value is reached at

a critical δ_H corresponding to the condition $\partial\overline{h}/\partial\delta_H = 0$, i.e., $\delta_H = 1/(2b)$ (see Equation 30). A further increase of the δ_H yields an increase of $\overline{h}$.

3 Study area and datasets

3.1 Overview of Lingdingyang Bay

The Pearl River (Figure 4a) delivered 2,823 $\times$ 10^8 m^3/yr of freshwater and 72.4 $\times$ 10^6 t/yr of suspended sediment load (Liu et al., 2014) into the South China Sea during the period from the 1950s to the 2000s via eight outlets, i.e., four eastern outlets (Humen, Jiaomen, Hongqili, Hengmen) and four western outlets (Modaomen, Jitimen, Yamen and Hutiaomen). Lingdingyang Bay is the largest estuary of the Pearl River Estuary, and mainly receives water and sediment inputs from the four eastern outlets (Figure 4b). Lingdingyang Bay is a funnel-shaped subaqueous delta and has a complicated geomorphology pattern with two deep channels (i.e., East and West Channels) between three shoals (i.e., East, Middle and West Shoals) (see Figure 4c). The tide in Lingdingyang Bay mainly ~~come~~ comes from the Pacific Ocean and has an irregular and semidiurnal character, with a mean tidal range between 1.0 and 1.7 m (Mao et al., 2004). Generally, tidal propagation in Lingdingyang Bay is affected by geometry (e.g., bank convergence), bottom topography and river discharge, among which the impact from river discharge is minor because the freshwater discharge is small compared to the amplitude of the tidal discharge. Hence, Lingdingyang Bay is a tide-dominated estuary~~owing to its dramatic volume for water bodies~~. In response to the typical funnel shape topography, the mean tidal range is considerably amplified when a tidal wave propagates along Lingdingyang Bay, increasing from 1.1 m at Chiwan (denoted by CW hereafter) near the mouth to approximately 3.2 m at Sishengwei (denoted by SSW hereafter) near the head of the bay, located 58 km upstream. The tidal wave is continuously amplified until Huangpu gauging station (24 km upstream from CW) with a mean tidal range of approximately 3.6 m, after which it is damped until vanishing (Cai et al., 2019).

In recent decades, intensive human activities (e.g., land reclamation, channel dredging, sand excavation and dam constructions) have substantially disturbed the natural morphological evolution of Lingdingyang Bay. In particular, land reclamation was usually done in areas shallower than approximately 0.5 m; thus, nearly 200 km^2 of land was reclaimed during 1988-2008 (Wu et al., 2014). In addition, after the initial dredging of the West channel to produce a navigation channel with a target depth of 6.9 m in 1959, several other dredging operations were conducted to maintain a specific depth (e.g., 8.6 m in 1980s). Since the 1990s, three stages of channel dredging were implemented in the West Channel in 2001, 2007 and 2012, with target depths of -11.5 m, -13.0 m, and -17.0 m (relative to the datum of lowest low water level, which is 1.7 m below mean sea level), respectively (Li, 2008). Furthermore, sand excavation is conducted in Lingdingyang Bay. According to Wu et al. (2016a), channel dredging and sand excavation caused local changes in the water depth of approxi-

mately 5 m/yr between 2012 and 2013. Moreover, large amount of sediments were trapped due to the operation of upstream reservoirs, which also exerts substantial influence on the morphological evolution in Lingdingyang Bay. It was shown by Wu et al. (2016a) that the volume of Lingdingyang Bay was dramatically increased during 2000-2010 owing to the combined influence of reduced sediment input, dredging and sand excavation.

3.2 Datasets

Bathymetric maps of Lingdingyang Bay with scales of 1:25,000, 1:50,000, and 1:75,000, surveyed in 1965, 1974, 1989, 1998, 2009 and 2015, were provided by the Guangzhou Maritime Safety Administration and China People's Liberation Army Navy Command Assurance Department of Navigation. The water depths, isobaths and estuarine outlines on these maps were digitalized in order to generate a digital elevation model (DEM) used to analyse the morphological changes of Lingdingyang Bay over ~50 years (from 1965 to 2015). Using the latitude/longitude information, they were then projected to UTM-WGS84 coordinates of China and interpolated to a 50 × 50 m grid DEM with kriging interpolation in ArcGIS, which was extensively applied to analyze the evolution of morphological changes (e.g., Brunier et al., 2014; Liu et al., 2019).

To explore the tidal hydrodynamics in Lingdingyang Bay, tidal water level records (see Figure 5 for the records in January, the records in other months were not presented) for the periods with surveyed bathymetric maps were obtained from the Ministry of Water Resources of China (MWRC). These observations were taken at the CW and SSW gauging stations (see their locations in Figure 4) and were used to have a first estimate of wave celerity (Equation 26) and the tidal damping ~~/amplificationrate~~ (or amplification) rate (Equation 27) over the studied channel. From Figure 5, we observe that the tide in Lingdingyang Bay is characterized by a semi-diurnal mixed tidal regime with apparent daily inequality in range and time between high and low waters. As the tide propagates from CW to SSW, the tidal range is amplified due to the strong channel convergence. The collected tidal water level records generally contained two high and two low water levels for each day. These data were then interpolated to one hour intervals for harmonic analysis by using the shape preserving piecewise cubic interpolation. The tidal water levels derived from such an interpolation method can well retain the power spectra of low frequency bands and principal tides (e.g., M_2), while the high frequency bands may not be entirely reproduced (see a similar result in Zhang et al., 2018, using a trigonometric interpolation method).

Figure 6 shows the morphological changes in Lingdingyang Bay from 1965 to 2015. From 1965 to 1974, an area of 36.3 km^2 was reclaimed within the bay (see Table 1), extending the coastline southward towards the open sea (see Figure 6A1, 6A2 and 6B1) and reducing the surface water area by 36.3 km^2 (Table 1). The magnitude of bathymetric changes was mainly less than 1 m in the bay (Figure B1), with ~~the~~ a general dominance of deposition. The mean water depth only decreased by 0.09 m (Table 1), corresponding to a water volume decrease of 2.0×10^8 m^3 during this period (Table

1). From 1974 to 1989, land reclamation was the most intensive, resulting in an increase of land area (and decrease of water area) of 129.2 km^2. During this period, significant deepening, ranging from 1 to 5 m, occurred in the West Trough due to the dredging of the navigation channel. The mean water depth only increased by 0.08 m in Lingdingyang Bay. However, the water volume continued to decrease by 0.3×10^8 m^3 in relation to the decrease in water area. Since the 1990s, dredging for the maintenance of the navigation channel intensified. From 1998 to 2015, land reclamation continued to increase the land area and decrease the water area in Lingdingyang Bay (Table 1)~~;~~ ~~however~~. However, the mean water depth and water volume increased by 0.75 m and 5.1×10^8 m^3, respectively (Table 1), although Figures 6A4 and 6A5 show that the West Trough became narrower due to the expansion of the West Shoal from 1998 to 2009. From 2009 to 2015, the area of the Middle Shoal was reduced, and pits up to ~20 m deep occurred in its upper sector due to sand excavation (Figure 6B5). It is evident that the morphological evolution in Lingdingyang Bay has been significantly altered by human activities since the 1990s.

4 Results

4.1 Variabilities of wave celerity and the tidal damping ~~/~~(or amplification) rate

In this paper, the observed wave celerity is derived from the travelling time of both high and low water levels (see Equation 26), while the tidal ~~amplitude damping /amplification~~damping (or amplification) rate is computed according to Equation (27). To illustrate the spring-neap variabilities of tidal dynamics, Figure 7 shows the observed c and δ_H as a function of the tidal amplitude at the estuary mouth η_0 (i.e., CW station) for different years. In general, we observe that both wave celerity and the damping ~~/amplificationrate are decreased~~ (or amplification) rate decrease with increasing tidal amplitude at the estuary mouth with slightly different negative slopes (indicated by α ~~for the~~ and β representing the change rate of wave celerity and ~~β for tidal damping /amplification rate~~ tidal damping or amplification rate with respect to the tidal amplitude, respectively), suggesting a more strongly amplified yet faster wave for the neap tide ~~than that~~ (smaller η_0, larger δ_H and c) than for the spring tide (larger η_0, smaller δ_H and c). Furthermore, we observe a clear pattern of increasing average wave celerity over the period between 1965 and 2015 (Figures 7a-f), which corresponds to an increasing trend of the tidal amplification rate over the period. In addition, the spring-neap variability of tidal amplification is apparently large in 1965 and decreases until 2015.

Note that both the wave celerity and the tidal damping ~~/amplification~~(or amplification) rate reflect the imbalance between channel convergence and bottom friction (Savenije and Veling, 2005). It is evident from the definition of the friction number χ (see Equation 10) that effective bottom friction experienced for the spring tide is stronger than that for the neap tide due to a larger tidal amplitude to depth ratio ζ during the spring tide. On the other hand, the estuary shape number ~~γ~~ and the tidally averaged depth $\overline{h}$ are more or less the same for spring and neap tides. Hence, the tidal damping

/amplification(or amplification) rate experienced by the estuary is larger for the neap tide than that for the spring tide.

To investigate the underlying mechanism of such a spring-neap variability of wave celerity, we further rewrite the celerity Equation (19) by substituting Equation (12):

$$c = \frac{c_0}{\sqrt{1-\delta\,(\gamma-\delta)}}\,. \tag{31}$$

It is evident from Equation (31) that the wave celerity c is increased increases with the tidal damping /amplification(or amplification) number δ for given constant values of γ and $\overline{h}$. Hence, assuming a more or less constant tidally averaged depth over a spring-neap cycle, it is concluded that the wave celerity during the neap tide is generally faster than that during the spring tide.

4.2 Performance of analytical model for reproducing the tidal hydrodynamics

Before an inverse analytical model can be used to predict the morphological changes in estuaries, it is required to well calibrate and validate the model against observations. Hence, the analytical model presented in section 2.1 is used to reproduce the historic physical properties of the tidal wave (i.e., tidal damping /or amplification rate and wave celerity) in Lingdingyang Bay. The estuarine system is subject to a harmonic tide at the estuary mouth (i.e., CW station). In order to calibrate and validate the analytical model, the tidal properties (including the tidal amplitude and phase) of predominant M_2 tide at a monthly averaged scale were extracted by means of a classical harmonic analysis making use of T_TIDE MATLAB Toolbox provided by Pawlowicz et al. (2002). Based on the collected topographic maps (see details in section 3.2), the geometry of Lingdingyang Bay can be described by exponential functions (5)-(6) (Figure 8), and the fitted geometric characteristics are given in Table 2. In order to account for the along-channel variations of the estuarine sections, we adopted a longitudinal variable depth along the channel. In Figure 8, we also observe a sudden decrease of cross-sectional area near the Humen outlet, which is due to the strong width convergence towards the rock-bound gorges with a relatively greater larger water depth.

In Figure 9, the analytically computed tidal amplitude η (see Equation 24) and phase ϕ_Z (see Equation 20) of the predominant M_2 tide at SSW (x=58 km) are compared with the observed values in Lingdingyang Bay for different years. We calibrated the analytical model by adjusting the Manning-Strickler friction coefficient K and the storage width ratio r_S, which are detailed in Table 3. In particular, the calibrated r_S is relatively sensitive to the variation in phase of the elevation. In addition, it is worth noting that in the analytical model the calibrated Manning-Stricker friction coefficient K should be regarded as an equivalent effective friction coefficient induced by the entire estuary, including the additional drag resistance due to bed forms, the influence of suspended sediments and the possible effect due to lateral storage areas (Cai et al., 2016). The model performance was evaluated by the root mean squared error (RMSE), where RMSE=0 corresponds to

perfect agreement. In general, the correspondence between analytical results and observations is good, both for the tidal amplitude (with RMSE ranging between 0.015 and 0.020 m) and the phases (with RMSE ranging between 1.1° and 2.1°), suggesting that the analytical model can reproduce the main tidal hydrodynamics in Lingdingyang Bay well. The calibrated friction coefficient K ranges between 58 $m^{1/3}s^{-1}$ and 90 $m^{1/3}s^{-1}$, with ~~the~~ a minimum value occurring in 2009 (indicating relatively strong friction) and ~~the~~ a maximum in 1965 (indicating relatively weak friction). On the other hand, the calibrated storage width ratio r_S is approximately unit (ranging between 1.0 and 1.15), which suggests a minor impact from the lateral storage areas on the evolution of tidal hydrodynamics.

Subsequently, the analytically computed tidal characteristics of Lingdingyang Bay were used to describe how the tidal hydrodynamics are affected by the morphological evolution. In Figure 10, the diagrams of the velocity number μ, damping number δ, celerity number γ and phase lag ε are shown together with the trajectory of their corresponding dimensionless parameters in Lingdingyang Bay. It is worth noting that the longitudinal estuary shape number γ decreased in 1965, 1974 and 1989 due to the shallowing of the estuary in the landward direction. Conversely, we observe an increased γ in 2009 and 2015, which is due to the increased depth in the channel (see Figure 8). In these graphs, the longitudinal variations of the four dimensionless dynamics for different years are represented by different colours, where square symbols represent the initial position of CW station, while the circular symbols represent the position of SSW station. In Figure 10, we can clearly see a transition in the hydrodynamics pattern during the studied period (1965-2015). Both the averaged values of the velocity number and damping/amplification number tend to decrease from 1965 to 1989, after which the values recover and approach the status in the 1960s. Figure 10c shows a similar picture for the celerity number, except that the values tend to increase from 1965 to 2015. In contrast, the longitudinal variation of phase lag displays a consistent decreasing tendency, which suggests that the tidal wave shows a more standing wave character with larger value of phase difference between velocity and elevation. Table 4 presents the spatially averaged values of the main dimensionless parameters over 1965-2015, where we see a clear transition pattern that occurs approximately around 1989. From the physical point of view, it can be seen that the tidal hydrodynamics become weak during the period of 1965-1989 (indicating lower values of μ and δ), after which the hydrodynamics becomes stronger in recent years (indicating larger values of μ and δ).

4.3 Estimation of the tidally averaged depth

The successful reproduction of tidal hydrodynamics using an analytical model suggests a close relationship between tidal damping ~~/amplification~~(or amplification) and wave celerity, which can be described by the celerity Equation (19). Thus, it is possible to develop an inverse analytical model to estimate the tidally averaged depth $\overline{h}$ for given observed wave celerity and the tidal damping ~~/amplification~~(or amplification) rate from observed water levels, as presented in section 2.2. In this

case, we assume a constant depth, and hence, the width convergence length equals to the cross-sectional area length, i.e., $a = b$.

We adopted the width convergence length from topographic maps and estimated wave celerity and tidal damping ~~/amplification~~(or amplification) from the observed water levels. Combining these parameters with the calibrated storage width ratio r_S (see Table 3), Equation (25) can be used for a first estimate of the tidally averaged depth. Figure 11 shows the observed wave celerity and tidal damping ~~/amplification~~(or amplification) together with the estimated tidally averaged depth and tidal amplitude at the CW station over the studied period. The monthly variation in estimated depth is mainly due to the change in mean sea level. In particular, we see a very similar variability of the derived depth with that of the wave celerity, which suggests a stronger influence of wave celerity when compared with the tidal amplification in Lingdingyang Bay.

Figure 12 shows the analytically computed tidally averaged depth and water volume at an annual scale in Lingdingyang Bay in different years. Note that in Figure 12, the annual mean storage width ratio r_S and water area of Lingdingyang Bay were obtained by means of the shape preserving piecewise cubic interpolation based on the calibrated and observed values, respectively. Here, the observed depth and water volume refer to the values relative to mean sea level, since the analytical model is derived based on a tidally averaged scale. For both geometric characteristics, the agreement with observations is reasonably good, with RMSE of 0.068 m and $0.61*10^8$ m^3, respectively. This suggests that the proposed method can be a useful tool to have a first estimate of the morphological evolution in terms of depth and volume.

5 Discussions

5.1 Influence of the morphological evolution on tidal hydrodynamics

Lingdingyang Bay is a typical funnel-shaped estuary, where the tidal dynamics are one of the main factors maintaining the stability state of estuarine morphology. Generally, the tides in the Pearl River Estuary are influenced by the geometry (i.e., cross-sectional variation) and river discharge (Zhang et al., 2010). The water discharge ~~shows~~ has shown insignificant change since the 1950s (Liu et al., 2017)~~; therefore~~. Therefore, morphological changes became the main factors influencing the tidal dynamics of Lingdingyang Bay. Due to land reclamation, the water area and water volume of Lingdingyang Bay decreased from 1965 to 1974. Since the 1980s, channel dredging was conducted in the West Trough (i.e., Lingdingyang Channel) (Wu et al., 2016a), and the West Trough became deeper from 1974 to 1989 (Figure 5B2). Therefore, although land area in Lingdingyang Bay increased by 30.5% from 1974 to 1989, water volume only decreased by 0.8%, and the mean water depth increased by 0.08 m (Table 1). In addition, since 1989, the mean water depth has increased significantly because of intensive channel dredging and reduced sediment inputs (due to reservoirs operation in the Pearl River basin) in Lingdingyang Bay. Hence, it seems that the morphological

evolution pattern of Lingdingyang Bay has changed since 1989. Correspondingly, temporal changes in the tidal dynamics of Lingdingyang Bay show that the tidal dynamics pattern has also changed since 1989 (see Figures 7, 9,10 and Table 4).

To better understand the response of the morphological evolution to tidal dynamics, we rewrite the equilibrium depth h_I (subscript I indicates ideal estuary) through Equation (18) for the case of an ideal estuary, where $\delta = 0$:

$$h_I = \left(\frac{8}{3\pi K^2} \upsilon b \sqrt{g} \right)^{6/11} . \tag{32}$$

~~which~~ This shows that the equilibrium depth h_I is inversely proportional to the Manning-Strickler friction coefficient K with the power of 12/11, while it is proportional to the velocity amplitude υ with the power of 6/11. If we assume a more or less constant width convergence length, then the response of the morphological evolution can be inferred from the combined impacts from the Manning-Strickler friction coefficient (representing the bottom friction) and velocity amplitude (representing the tidal dynamics). Specifically, we observed a decreasing trend of calibrated K during 1965-1989, while there was an increasing trend during 1989-2015 (see Table 3). This suggests that the tidally averaged depth tends to increase before the 1990s, after which it would decrease again. However, we actually observed a consistent increase of water depth over the studied period, which has to do with the alteration of the tidal dynamics, especially due to the velocity amplitude. In Table 4, it can be seen that the dimensionless velocity number μ decreased from 1965 to 1989 (indicating a decrease trend of water depth), after which it increased until 2015 (indicating an increase trend of water depth). Hence, for the period of 1965-1989, the potential impact from bottom friction on morphological evolution dominated over the alteration of tidal dynamics. In contrast, the observed channel deepening in the following decades is mainly controlled by the reinforced tidal dynamics that has dominated over the bottom friction.

5.2 Model limitations

It should be noted that several assumptions are made in order to derive the analytical solutions for tidal hydrodynamics. The fundamental assumption is that the tidal amplitude to depth ratio and the Froude number are considerably smaller than unity so that the linearized St. Venant equations can be used for the derivations. A second fundamental assumption is that both the cross-sectional area and width can be described by exponential functions, following Equations (5) and (6), as is the case for most alluvial estuaries. We also assume that the cross section is most rectangular, with a possible impact from lateral storage area described by the storage width ratio r_S. In this study, the r_S values were obtained by calibration against the extracting harmonic constants for given geometries observed in Lingdingyang Bay. For a fully predictive model, additional satellite maps (such as archived Landsat MSS/TM data, http://glovis.usgs.gov/) at different periods (i.e., the spring tide and

moderate tide) are required to help define the intertidal zone (and hence the r_S value). In addition, we neglect the influence of river discharge on tidal dynamics, which is not such a restriction in the downstream part of alluvial estuaries where the river flow velocity is small compared to the tidal velocity. It was shown that the tidally averaged depth varies due to the nonlinear residual friction effect (e.g., Cai et al., 2014). By using a harmonic solution, the residual water level slope along the channel is assumed to be null, which means that the model cannot reproduce the spring-neap change of the tidally averaged depth along the channel, although the depth is usually larger during the spring tide (and also during the flood season) than during the neap tide (and also during the dry season) in tide-dominated estuaries. Moreover, by adopting an analytical solution for tidal hydrodynamics in an infinitely long channel, the model excludes the impact of reflected waves from the closed end on tidal dynamics. Therefore, the proposed analytical approach is preferably applied to tidally dominated estuaries (or bays) free of tidal barriers or sluices at the upstream end, and where the tide dominates over the river discharge.

6 Conclusions

In this paper, a novel approach for estimating the tidally averaged depth was proposed to understand the morphological evolution based on the observed water levels at 2 stations (at least) in estuaries. The linear analytical hydrodynamics model proposed by Cai et al. (2012) was used to explore the hydrodynamics changes in Lingdingyang Bay, where we observe an evident hydrodynamics pattern transition due to the substantial changes of morphology. The analytically computed tidal amplitude and travelling time are compared to the observations, and the correspondence is good, which suggests that the proposed model can be a useful method for analysing the changes of physical tidal properties along the channel. Conversely, for given observed tidal water levels, it is possible to have a first estimate of wave celerity and tidal damping ~~/amplification~~(or amplification) rate, and subsequently the tidally averaged depth and other tidal properties (e.g., velocity amplitude, phase lag), by manipulating the set of Equations (16)-(19). Thus, the proposed method could be particularly useful in situations where there are not sufficient data (e.g., detailed navigational charts) available, while a first estimate of estuary depth and water volume are required.

Data availability. The data and source codes used to reproduce the experiments presented in this paper are available from the authors upon request (caihy7@mail.sysu.edu.cn).

Author contributions. All authors contributed to the design and development of the work. The experiments were originally carried out by HC. PZ, SH carried out the data analysis. FL and HC prepared the paper with contributions from all co-authors. EG, PM and QY reviewed the paper.

Competing interests. The authors declare that they have no conflict of interest.

Acknowledgements. We acknowledge the financial support from the National Key R&D of China (Grant

No. 2016YFC0402601), from the National Natural Science Foundation of China (Grant No. 51979296, 51709287, 41706088, 41476073), from the Fundamental Research Funds for the Central Universities of China (No.18lgpy29) and from the Water Resource Science and Technology Innovation Program of Guangdong Province (Grant No. 2016-20, 2016-21). The work of the third author was supported by FCT research contract IF/00661/2014/CP1234.

Appendix A

Scaling the governing equations

We introduce a scaling on Equations (2) and (3), similar to that used by Savenije et al. (2008), to derive the dimensionless equations, with the asterisk superscript denoting dimensionless variables:

$$U^* = U/\upsilon_0,\ h^* = h/\overline{h},\ Z^* = Z/\eta_0,\ x^* = x\frac{2\pi}{L},\ t^* = t\frac{2\pi}{T}\,, \tag{A1}$$

where η_0 and υ_0 are the tidal amplitude and velocity amplitude at the estuary mouth, L is the wavelength and T is the tidal period. Note that the scaling of tidal flow velocity and water level fluctuation are slightly different from the scaling used by Savenije et al. (2008) because they are scaled with the corresponding values at the estuary mouth. For an infinite length estuary, the velocity amplitude and the tidal amplitude are proportional:

$$\frac{1}{\upsilon}\frac{\partial \upsilon}{\partial x} = \frac{1}{\eta}\frac{\partial \eta}{\partial x}\,, \tag{A2}$$

which implies that the ratio of the velocity amplitude to the tidal amplitude is constant:

$$\frac{\upsilon}{\eta} = \frac{\upsilon_0}{\eta_0}\,. \tag{A3}$$

Making use of the assumption (A3), equations (2) and (3) may then be rewritten as:

$$\frac{\partial Z^*}{\partial t^*} + \left(\frac{\overline{h}\upsilon T}{\eta L r_S}\right) h^* \frac{\partial U^*}{\partial x^*} - \left(\frac{\overline{h}\upsilon T}{2\pi\eta b r_S}\right) h^* U^* = 0\,, \tag{A4}$$

$$\frac{\partial U^*}{\partial t^*} + \left(\frac{g\eta T}{\upsilon L}\right)\frac{\partial Z^*}{\partial x^*} + \left(r\frac{T}{2\pi\overline{h}}\right) U^* = 0\,. \tag{A5}$$

The real scales of velocity amplitude υ and wavelength L are scaled with the corresponding values for a frictionless tidal wave in a channel with zero convergence (U_0, L_0) as a reference:

$$\upsilon = U_0\mu\,, \tag{A6}$$

$$L = L_0/\lambda\,, \tag{A7}$$

where we introduce the unknown dimensionless velocity number μ and celerity number λ.

For the case of a frictionless estuary with zero convergence, the classical wave celerity c_0 is defined by (1), while the velocity amplitude U_0 and the wavelength L_0 are:

$$U_0 = \zeta c_0 r_S\,, \tag{A8}$$

$$L_0 = c_0 T\,, \tag{A9}$$

where ζ represents the dimensionless tidal amplitude to depth ratio (see Equation (15)).

Assuming $h^* = 1$ (i.e., $h = \overline{h}$) in the continuity Equation (A4), then the dimensionless Equations (A4) and (A5) read:

$$\frac{\partial z^*}{\partial t^*} + \mu\lambda\frac{\partial U^*}{\partial x^*} - \mu\gamma U^* = 0\,, \tag{A10}$$

$$\frac{\partial U^*}{\partial t^*} + \frac{\lambda}{\mu}\frac{\partial z^*}{\partial x^*} + \frac{8}{3\pi}\mu\chi U^* = 0\,, \tag{A11}$$

where the dimensionless parameters γ and χ have been introduced as the estuary shape number (9) and the friction number (10), respectively, while the corresponding definitions of the velocity number μ and the celerity number λ are defined in (11) and (12), respectively.

Appendix B

Derivation of the tidally averaged water depth from an inverse analytical model

Introducing the dimensionless parameters (9), (12), (13) into the celerity equation (19) yields

$$\left(\frac{c_0}{c}\right)^2 = 1 - \frac{1}{\eta}\frac{\mathrm{d}\eta}{\mathrm{d}x}\frac{c_0}{\omega}\left(\frac{c_0}{\omega b} - \frac{1}{\eta}\frac{d\eta}{dx}\frac{c_0}{\omega}\right)\,, \tag{B1}$$

where a has been replaced by b in the definition of γ (9) due to the assumption of a horizontal bed.

Substitution of the classical wave speed $c_0 = \sqrt{g\overline{h}/r_S}$ (1) and the tidal damping rate δ_H (27) into Equation (B1), we end up with Equation (25) in the main text.

References

Brunier, G.and Anthony, E. J., Goichot, M., and Provansal, M.and Dussouillez, P.: Recent morphological changes in the Mekong and Bassac river channels, Mekong delta: the marked impact of river-bed mining and implications for delta destabilisation, Geomorphology, 224, 177–191, doi:10.1016/j.geomorph.2014.07.009, 2014.

Cai, H., Savenije, H. H. G., and Toffolon, M.: A new analytical framework for assessing the effect of sea-level rise and dredging on tidal damping in estuaries, Journal of Geophysical Research-Oceans, 117, C09 023, doi:Artn C09023 10.1029/2012jc008000, 2012.

Cai, H., Savenije, H. H. G., and Jiang, C.: Analytical approach for predicting fresh water discharge in an estuary based on tidal water level observations, Hydrology and Earth System Sciences, 18, 4153–4168, doi:10.5194/hess-18-4153-2014, 2014.

Cai, H., Toffolon, M., and Savenije, H. H. G.: An Analytical Approach to Determining Resonance in Semi-Closed Convergent Tidal Channels, Coastal Engineering Journal, 58, 1650 009, doi:Artn 1650009 10.1142/S0578563416500091, 2016.

Cai, H., Huang, J., Niu, L., Ren, L., Liu, F., Ou, S., and Yang, Q.: Decadal variability of tidal dynamics in the Pearl River Delta: Spatial patterns, causes, and implications for estuarine water management, Hydrological Processes, 32, 3805–3819, doi:10.1002/hyp.13291, 2019.

Deng, J. and Bao, Y.: Morphologic evolution and hydrodynamic variation during the last 30 years in the LINGDING Bay, South China Sea, Journal of Coastal Research, pp. 1482–1489, 2011.

Du, J. L., Yang, S. L., and Feng, H.: Recent human impacts on the morphological evolution of the Yangtze River delta foreland: A review and new perspectives, Estuarine Coastal and Shelf Science, 181, 160–169, doi:10.1016/j.ecss.2016.08.025, 2016.

Friedrichs, C. T. and Aubrey, D. G.: Tidal Propagation in Strongly Convergent Channels, Journal of Geophysical Research-Oceans, 99, 3321–3336, doi:10.1029/93jc03219, 1994.

Gisen, J. and Savenije, H. H. G.: Estimating bankfull discharge and depth in ungauged estuaries, Water Resources Research, 564, 2298–2316, doi:10.1002/2014WR016227, 2015.

Gong, W. and Shen, J.: The response of salt intrusion to changes in river discharge and tidal mixing during the dry season in the Modaomen Estuary, China, Continental Shelf Research, 31, 769–688, doi:10.1016/j.csr.2011.01.011, 2011.

Guo, L., van der Wegen, M., Roelvink, J. A., and He, Q.: The role of river flow and tidal asymmetry on 1-D estuarine morphodynamics, Journal of Geophysical Research-Earth Surface, 119, 2315–2334, doi:10.1002/2014JF003110, 2014.

Guo, L. C., van der Wegen, M., Wang, Z. B., Roelvink, D., and He, Q.: Exploring the impacts of multiple tidal constituents and varying river flow on long-term, large-scale estuarine morphodynamics by means of a 1-D model, Journal of Geophysical Research-Earth Surface, 121, 1000–1022, doi:10.1002/2016JF003821, 2016.

Hoitink, A. J. F., Wang, Z. B., Vermeulen, B., Huismans, Y., and Kastner, K.: Tidal controls on river delta morphology, Nature Geoscience, 10, 637–645, doi:10.1038/NGEO3000, 2017.

Jay, D. A.: Green Law Revisited - Tidal Long-Wave Propagation in Channels with Strong Topography, Journal of Geophysical Research-Oceans, 96, 20 585–20 598, doi:10.1029/91jc01633, 1991.

Jiang, C., Pan, S. Q., and Chen, S. L.: Recent morphological changes of the Yellow River

(Huanghe) submerged delta: Causes and environmental implications, Geomorphology, 293, 93–107, doi:10.1016/j.geomorph.2017.04.036, 2017.

Li, W.: Numerical modeling of tidal current on deep water channel project of Nansha Harbor District of Guangzhou Port, Journal of Waterway and Harbor, 29, 179–184 (in Chinese), 2008.

Liu, F., Yuan, L., Yang, Q., Ou, S. Y., Xie, L., and Cui, X.: Hydrological responses to the combined influence of diverse human activities in the Pearl River delta, China, Catena, 113, 41–55, doi:10.1016/j.catena.2013.09.003, 2014.

Liu, F., Chen, H., Cai, H. Y., Luo, X. X., Ou, S. Y., and Yang, Q. S.: Impacts of ENSO on multi-scale variations in sediment discharge from the Pearl River to the South China Sea, Geomorphology, 293, 24–36, doi:10.1016/j.geomorph.2017.05.007, 2017.

Liu, F., Xie, R., Luo, X., Yang, L., Cai, H., and Yang, Q. S.: Stepwise adjustment of deltaic channels in response to human interventions and its hydrological implications for sustainable water managements in the Pearl River Delta, China, Journal of Hydrology, 573, 194–206, doi:10.1016/j.jhydrol.2019.03.063, 2019.

Lorentz, H. A.: Verslag Staatscommissie Zuiderzee (in Dutch), Tech. rep., Alg. Landsdrukkerij, 1926.

Luan, H. L., Ding, P. X., Wang, Z. B., and Ge, J. Z.: Process-based morphodynamic modeling of the Yangtze Estuary at a decadal timescale: Controls on estuarine evolution and future trends, Geomorphology, 290, 347–364, doi:10.1016/j.geomorph.2017.04.016, 2017.

Mao, Q. W., Shi, P., Yin, K. D., Gan, J. P., and Qi, Y. Q.: Tides and tidal currents in the Pearl River estuary, Continental Shelf Research, 24, 1797–1808, doi:10.1016/j.csr.2004.06.008, 2004.

Monge-Ganuzas, M., Cearreta, A., and Evans, G.: Morphodynamic consequences of dredging and dumping activities along the lower Oka estuary (Urdaibai Biosphere Reserve, southeastern Bay of Biscay, Spain), Ocean & Coastal Management, 77, 40–49, doi:10.1016/j.ocecoaman.2012.02.006, 2013.

Pawlowicz, R., Beardsley, B., and Lentz, S.: Classical tidal harmonic analysis including error estimates in MATLAB using T-TIDE, Computers & Geosciences, 28, 929–937, doi:Pii S0098-3004(02)00013-4 Doi 10.1016/S0098-3004(02)00013-4, 2002.

Prandle, D.: How tides and river flows determine estuarine bathymetries, Progress in Oceanography, 61, 1–26, doi:10.1016/j.procean.2004.03.001, 2004.

Prandle, D. and Rahman, M.: Tidal Response in Estuaries, Journal of Physical Oceanography, 10, 1552–1573, doi:10.1175/1520-0485(1980)010⟨1552:TRIE⟩2.0.CO;2, 1980.

Savenije, H. H. G.: Salinity and Tides in Alluvial Estuaries, Elsevier, New York, 2005.

Savenije, H. H. G.: Salinity and Tides in Alluvial Estuaries, completely revised 2nd edition, www.salinityandtides.com, 2012.

Savenije, H. H. G. and Veling, E. J. M.: Relation between tidal damping and wave celerity in estuaries, Journal of Geophysical Research-Oceans, 110, doi:Artn C04007 10.1029/2004jc002278, 2005.

Savenije, H. H. G., Toffolon, M., Haas, J., and Veling, E. J. M.: Analytical description of tidal dynamics in convergent estuaries, Journal of Geophysical Research-Oceans, 113, doi:Artn C10025 10.1029/2007jc004408, 2008.

Schuttelaars, H. M., de Jonge, V. N., and Chernetsky, A.: Improving the predictive power when modelling physical effects of human interventions in estuarine systems, Ocean & Coastal Management, 79, 70–82, doi:10.1016/j.ocecoaman.2012.05.009, 2013.

Syvitski, J. P. M., Kettner, A. J., Overeem, I., Hutton, E. W. H., Hannon, M. T., Brakenridge, G. R., Day, J., Vorosmarty, C., Saito, Y., Giosan, L., and Nicholls, R. J.: Sinking deltas due to human activities, Nature Geoscience, 2, 681–686, doi:10.1038/NGEO629, 2009.

Toffolon, M. and Savenije, H. H. G.: Revisiting linearized one-dimensional tidal propagation, Journal of Geophysical Research-Oceans, 116, doi:Artn C07007 10.1029/2010jc006616, 2011.

van Maren, D. S., Oost, A. P., Wang, Z. B., and Vos, P. C.: The effect of land reclamations and sediment extraction on the suspended sediment concentration in the Ems Estuary, Marine Geology, 376, 147–157, doi:10.1016/j.margeo.2016.03.007, 2016.

van Rijn, L. C.: Analytical and numerical analysis of tides and salinities in estuaries; part I: tidal wave propagation in convergent estuaries, Ocean Dynamics, 61, 1719–1741, doi:10.1007/s10236-011-0453-0, 2011.

Wang, Z. B., Van Maren, D. S., Ding, P. X., Yang, S. L., Van Prooijen, B. C., De Vet, P. L. M., Winterwerp, J. C., De Vriend, H. J., Stive, M. J. F., and He, Q.: Human impacts on morphodynamic thresholds in estuarine systems, Continental Shelf Research, 111, 174–183, doi:10.1016/j.csr.2015.08.009, 2015.

Winterwerp, J. C. and Wang, Z. B.: Man-induced regime shifts in small estuaries-I: theory, Ocean Dynamics, 63, 1279–1292, doi:10.1007/s10236-013-0662-9, 2013.

Wu, C. S., Yang, S. L., Huang, S. C., and Mu, J. B.: Delta changes in the Pearl River estuary and its response to human activities (1954-2008), Quaternary International, 392, 147–154, doi:10.1016/j.quaint.2015.04.009, 2016a.

Wu, Z. Y., Milliman, J. D., Zhao, D. N., Zhou, J. Q., and Yao, C. H.: Recent geomorphic change in LingDing Bay, China, in response to economic and urban growth on the Pearl River Delta, Southern China, Global and Planetary Change, 123, 1–12, doi:10.1016/j.gloplacha.2014.10.009, 2014.

Wu, Z. Y., Saito, Y., Zhao, D. N., Zhou, J. Q., Cao, Z. Y., Li, S. J., Shang, J. H., and Liang, Y. Y.: Impact of human activities on subaqueous topographic change in Lingding Bay of the Pearl River estuary, China, during 1955-2013, Scientific Reports, 6, doi:Artn 37742 10.1038/Srep37742, 2016b.

Zhang, W., Ruan, X. H., Zheng, J. H., Zhu, Y. L., and Wu, H. X.: Long-term change in tidal dynamics and its cause in the Pearl River Delta, China, Geomorphology, 120, 209–223, doi:10.1016/j.geomorph.2010.03.031, 2010.

Zhang, W., Xu, Y., Hoitink, A. J. F., Sassi, M. G., Zheng, J. H., Chen, X. W., and Zhang, C.: Morphological change in the Pearl River Delta, China, Marine Geology, 363, 202–219, doi:10.1016/j.margeo.2015.02.012, 2015.

Zhang, W., Cao, Y., Zhu, Y., Zheng, J., Ji, X., Xu, Y., Wu, Y., and Hoitink, A.: Unravelling the causes of tidal asymmetry in deltas, Journal of Hydrology, 564, 588–604, doi:10.1016/j.jhydrol.2018.07.023, 2018.

Table 1. Geometric characteristics observed in Lingdingyang Bay from 1965 to 2015.

Parameters	1965	1974	1989	1998	2009	2015
[a]Land area (km^2)	387.2	423.4	552.6	578.1	627.9	645.3
Water area (km^2)	1220.1	1183.8	1054.6	1029.2	979.3	962.0
[b]Water depth (m)	4.2	4.1	4.2	4.3	4.5	5.0
Water volume (10^8 m^3)	40.1	37.9	37.6	37.2	37.6	42.3

[a] Difference between land areas in different years indicates the area of land reclaimed during this period;

[b] Water depth was calculated below the datum of the lowest low water level, which is 1.7 m below mean sea level.

Table 2. Geometric characteristics of Lingdingyang Bay.

Year	1965	1974	1989	1998	2009	2015
$\overline{A_0}$ (10^5 m^2)	2.44	2.29	2.29	2.08	2.08	2.08
$\overline{B_0}$ (km)	40.34	37.79	37.79	37.79	37.79	37.77
a (km)	34.10	33.61	31.77	36.09	37.49	43.66
b (km)	55.67	52.98	42.46	39.8	36.75	36.11
$\overline{h_0}^*$ (m)	4.71	4.76	5.07	5.19	5.57	6.16

Table 3. Calibrated parameters used for the analytical model and the evaluation of its performance using RMSE.

Years		1965	1974	1989	1998	2009	2015
Calibrated parameters	r_S	1.12	1.05	1.15	1.02	1.0	1.0
	K ($m^{1/3}s^{-1}$)	90	85	65	62	58	61
RMSE	Tidal amplitude (m)	0.020	0.018	0.019	0.018	0.018	0.015
	Phase (°)	1.9	2.1	1.9	1.7	2.1	1.1

Table 4. Spatially averaged dimensionless parameters in Lingdingyang Bay (0-58 km).

Years	γ	χ	μ	δ	λ	ε
1965	1.32	0.74	0.72	0.19	0.87	41.92
1974	1.40	0.76	0.70	0.20	0.85	40.18
1989	1.46	0.96	0.64	0.14	0.87	37.21
1998	1.39	0.99	0.64	0.13	0.90	36.66
2009	1.40	0.89	0.66	0.21	0.86	34.47
2015	1.27	0.81	0.70	0.25	0.86	34.64

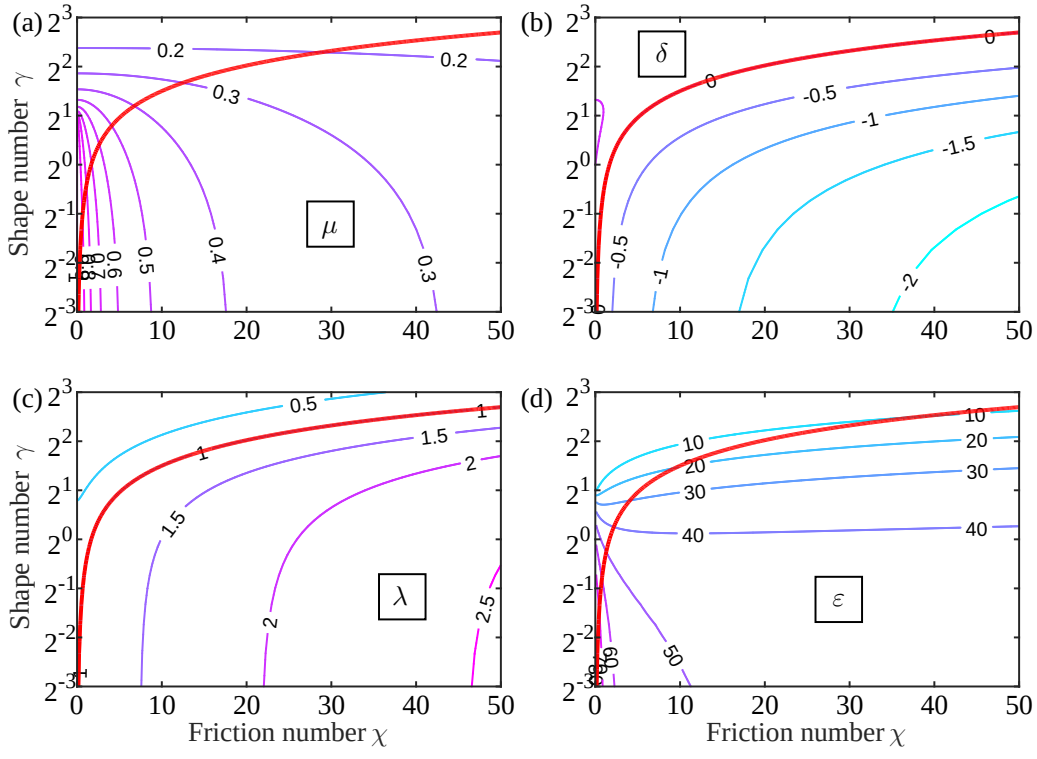

Fig. 1. Contour plot of the dimensionless dependent parameters (a: μ; b: δ; c: λ; d: ε) as a function of estuary shape number γ and friction number χ obtained with a linear model (Cai et al., 2012), in which thick red lines represent the ideal estuary, where $\delta = 0$, $\lambda = 1$, $\mu = 1/\sqrt{\gamma^2+1}$ and $\tan(\varepsilon) = 1/\gamma$.

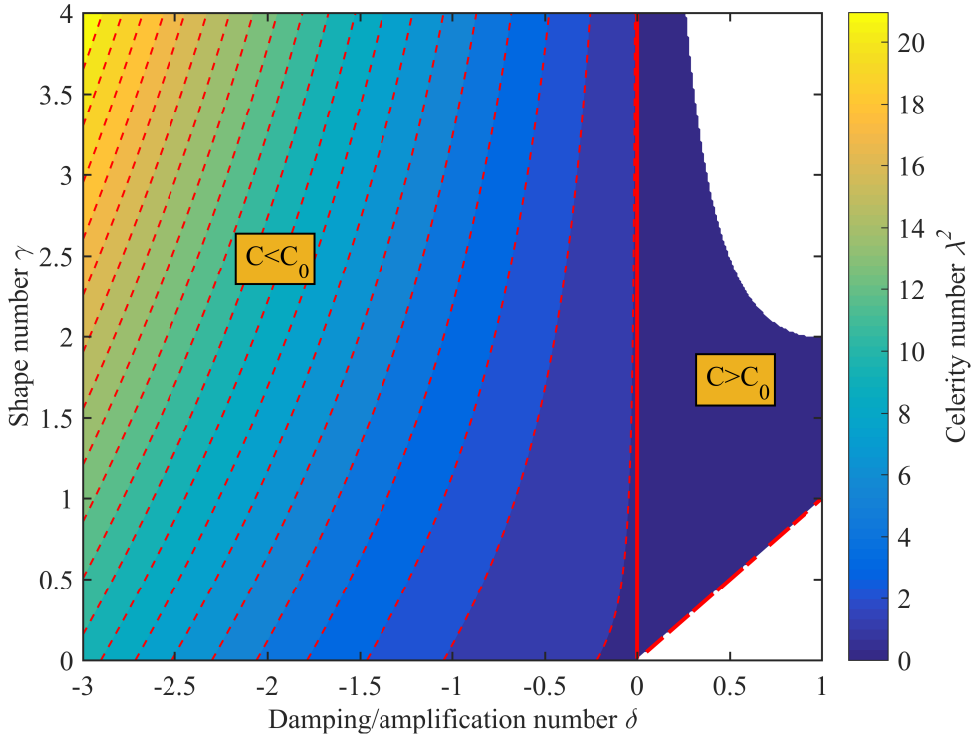

Fig. 2. Contour plot of the celerity number λ^2 as a function of estuary shape number γ and damping/amplification number δ obtained from Equation (19). The thick red line indicates the case of an ideal estuary ($\delta = 0$, $c = c_0$).

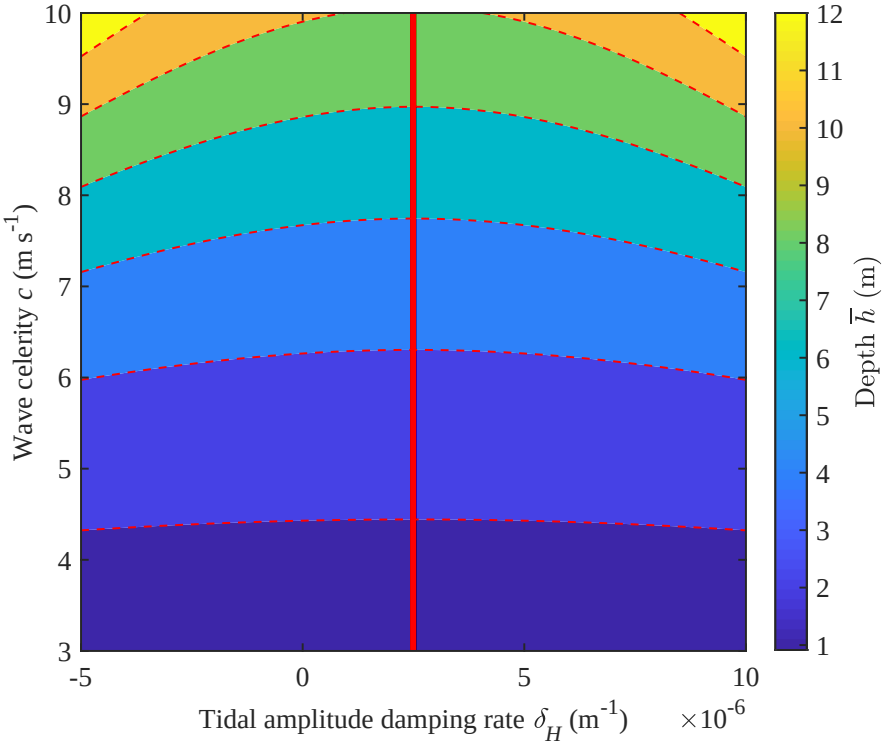

Fig. 3. Contour plot of the estimated depth $\overline{h}$ as a function of the wave celerity c and tidal ~~amplitude~~ damping (or amplification) rate δ_H obtained from Equation (25). The drawn red line indicates the critical value of $\delta_H = 1/(2b)$ corresponding to the minimum water depth for a given constant wave celerity.

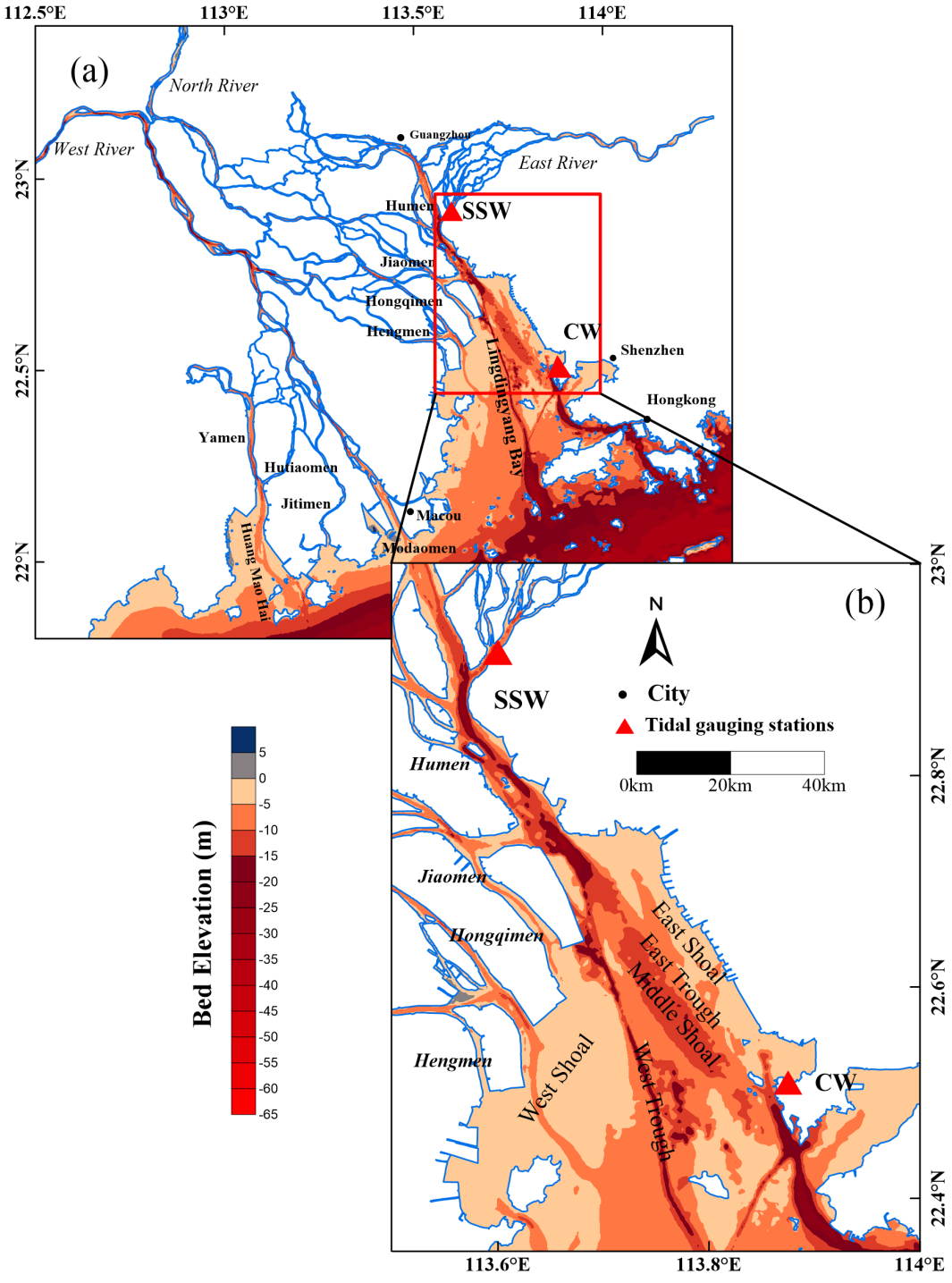

Fig. 4. Sketch of Lingdingyang Bay (b) in the Pearl River Estuary (a).

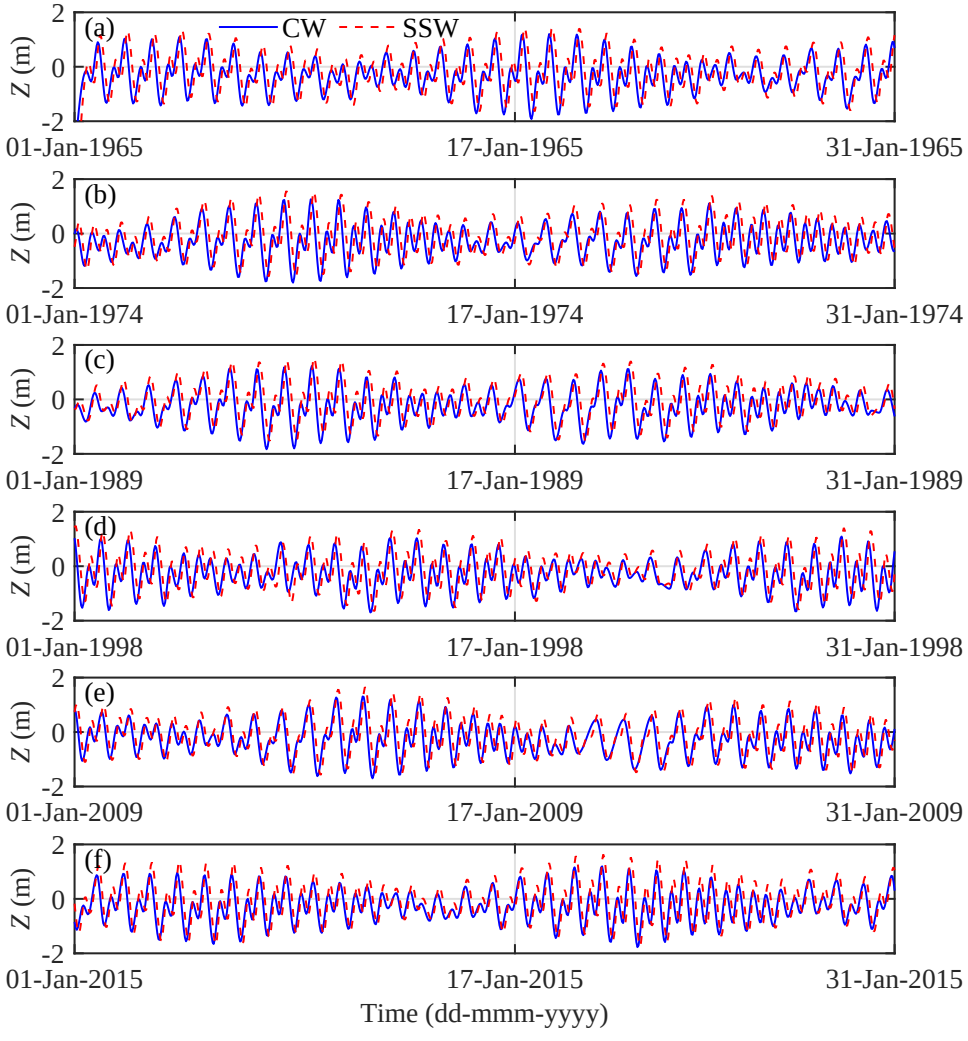

Fig. 5. Observed water levels (relative to mean sea level) in January for different periods: (a) 1965; (b) 1974; (c) 1989; (d) 1998; (e) 2009; (f) 2015.

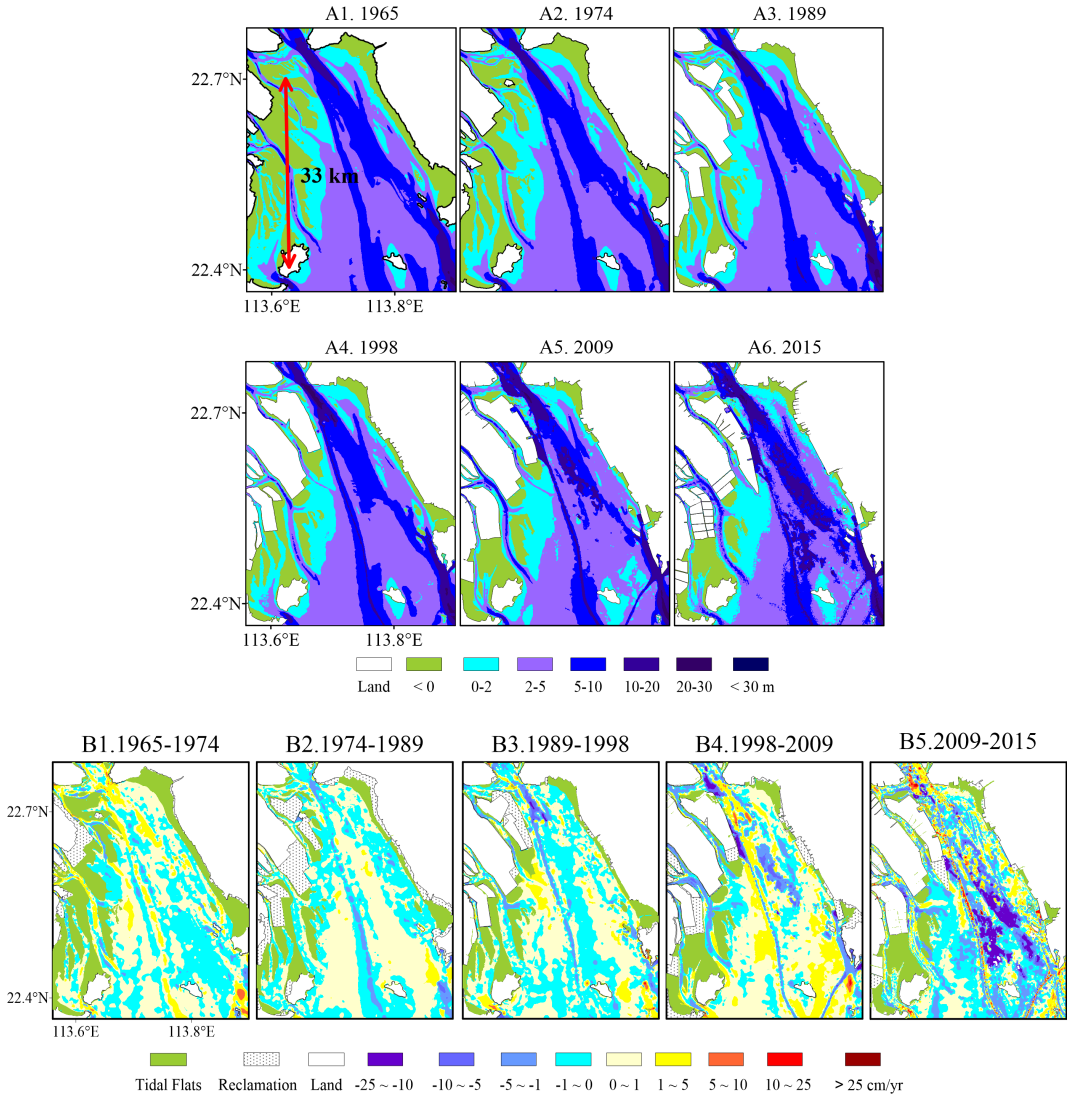

Fig. 6. Bathymetric maps of Lingdingyang Bay in 1965 (A1), 1974 (A2), 1989 (A3), 1998 (A4), 2009 (A5), and 2015 (A6) and its bathymetrical change rate during five time periods: 1965-1974 (B1), 1974-1989 (B2), 1989-1998 (B3), 1998-2009 (B4), and 2009-2015 (B5).

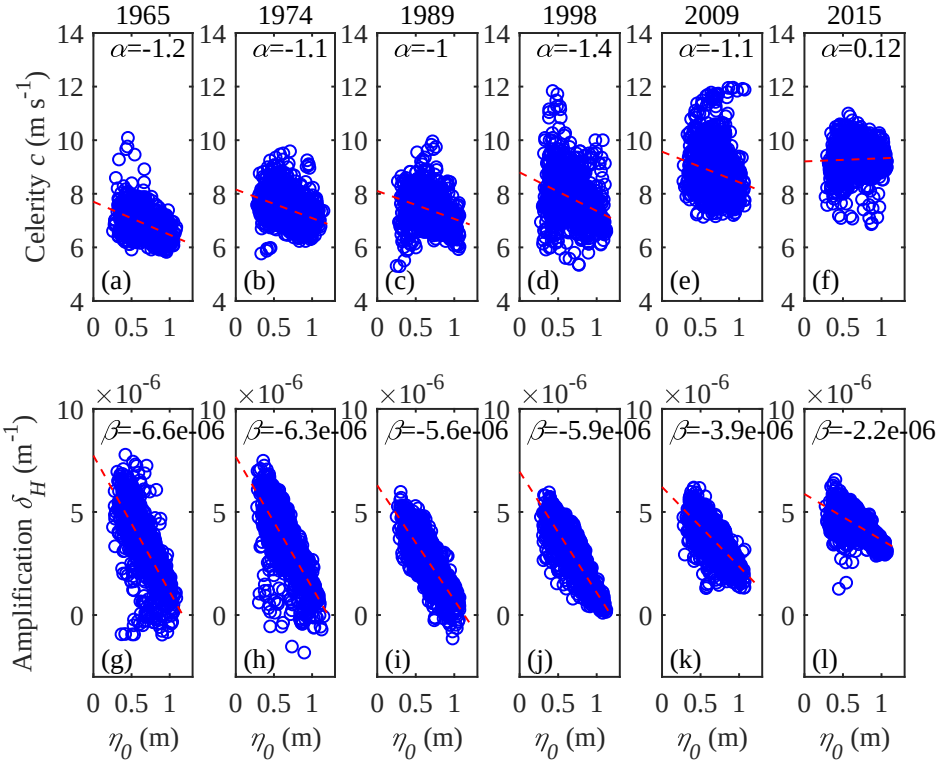

Fig. 7. Estimations of wave celerity c and tidal damping ~~/~~(or amplification) rate δ_H as a function of the tidal amplitude at the CW station η_0 in Lingdingyang Bay, in which the red line represents the best fit curve by linear regression with gradient of α for celerity and β for tidal amplification, respectively.

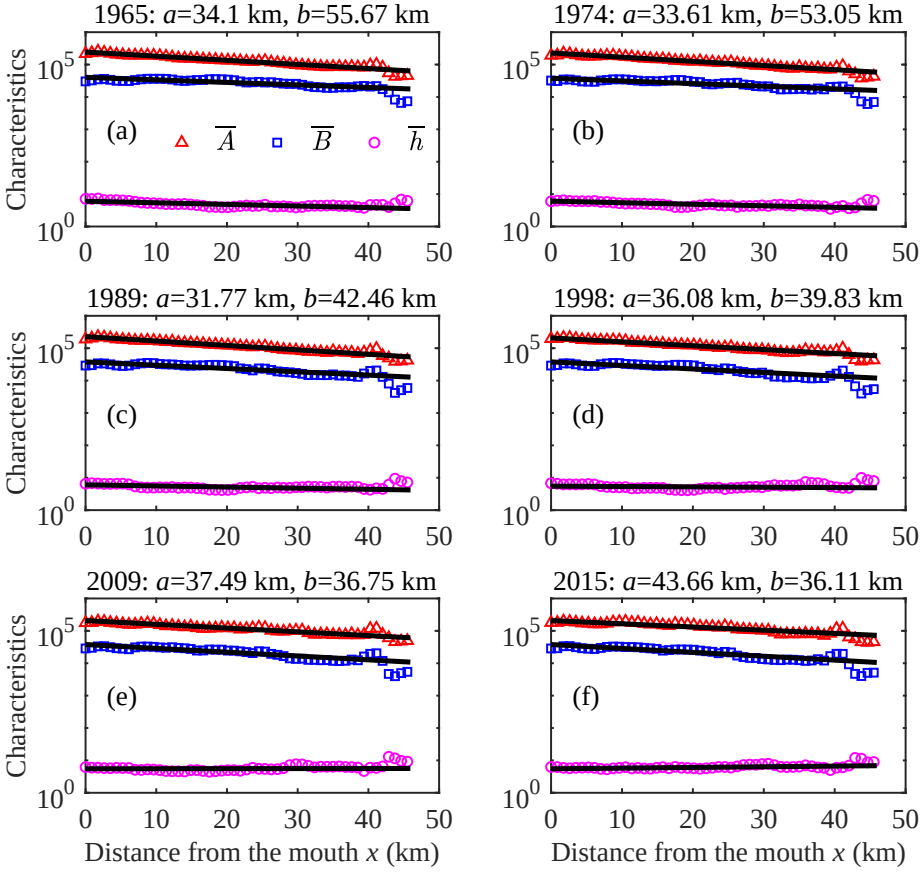

Fig. 8. Longitudinal variations of the geometric characteristics (the tidally averaged cross-sectional area $\overline{A}$, m^2, width $\overline{B}$, m, and depth $\overline{h}$, m) of Lingdingyang Bay for different years: a) 1965; b) 1974; c) 1989; d) 1998; e) 2009; and f) 2015, in which the black thin lines represent the best fitted curves according to the exponential functions (5)-(6).

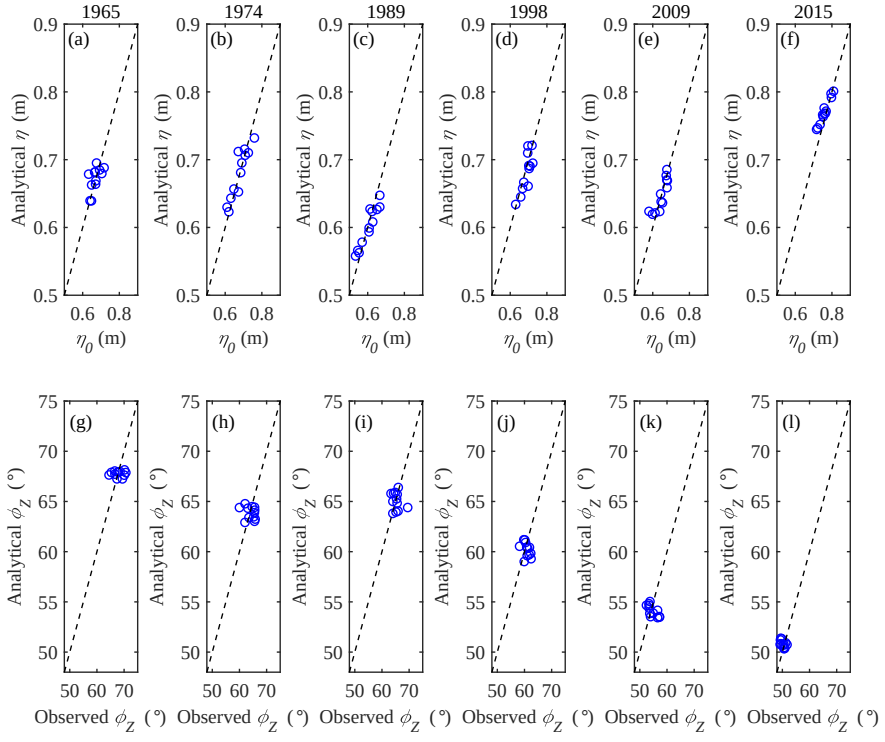

Fig. 9. Comparison between analytically computed tidal amplitude η (a, b, c, d, e, f) and phase ϕ_Z (g, h, i, j, k, l) with observations in Lingdingyang Bay for different years. The dashed line represents the perfect match between analytical results and observations.

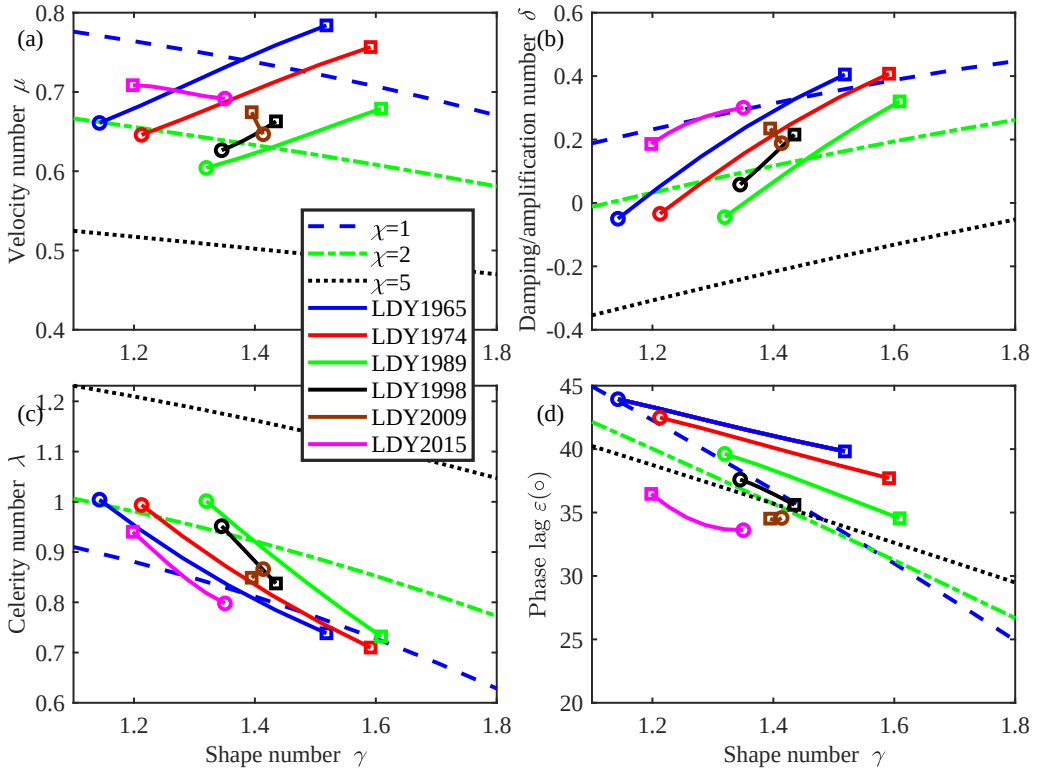

Fig. 10. Trajectories of the main dimensionless parameters as function of estuary shape number γ in Lingdingyang Bay (058 km) in: (a) velocity number diagram, (b) damping/amplification number diagram, (c) celerity number diagram, and (d) phase lag diagram. The square symbols indicate the initial position at CW station, while the circular symbols represent the final position at CW station. The background shows the lines of the hydrodynamics model with different values of the friction number χ.

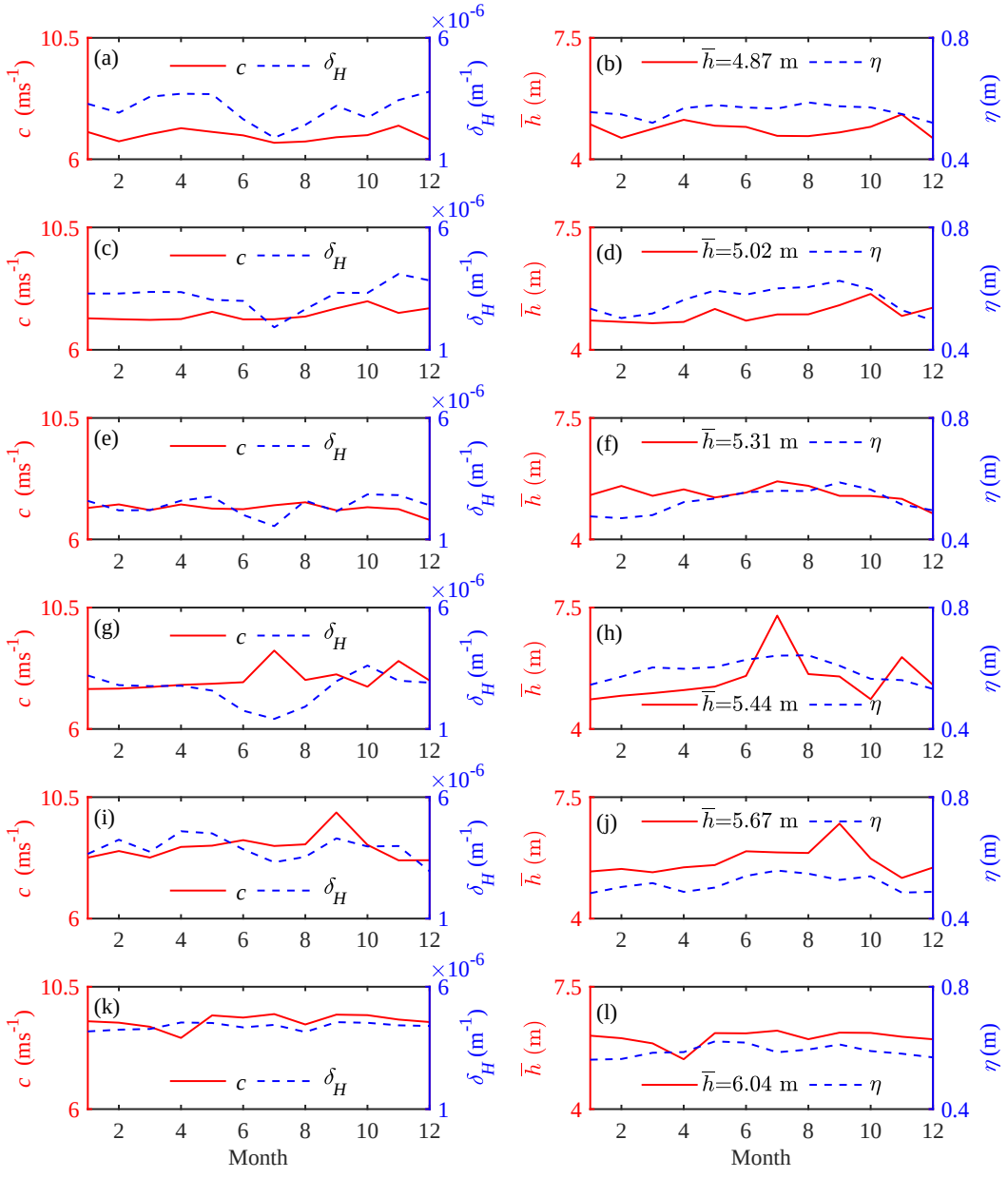

Fig. 11. Estimation of the tidally averaged depth $\overline{h}$ (the right panels, together with the tidal amplitude at the CW station η) using observed wave celerity c and tidal damping ~~/~~(or amplification) rate δ_H (the left panels) for different years: 1965 (a, b), 1974 (c, d), 1989 (e, f), 1998 (g, h), 2009 (i, j) and 2015 (k, l).

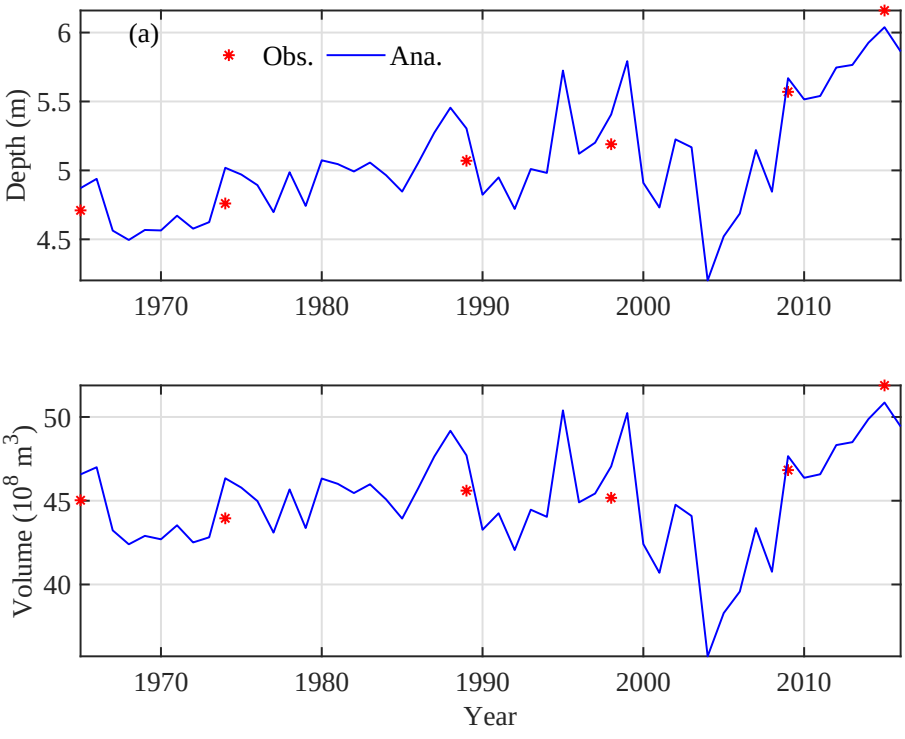

Fig. 12. Comparison between analytically computed tidally averaged depth (a) and volume (b) with observations in Lingdingyang Bay.